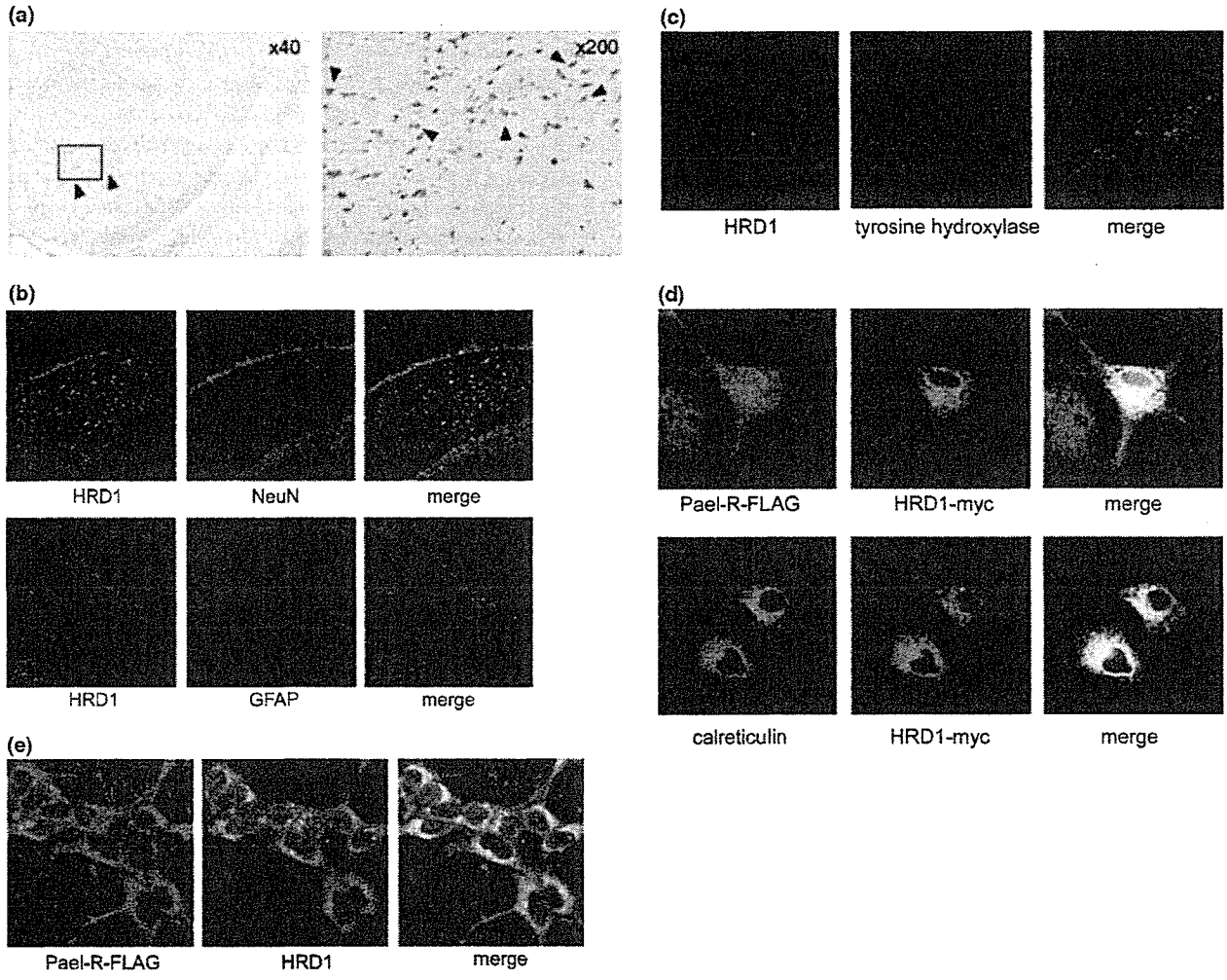

Fig. 1 Brain distribution and subcellular localization of Pael-R and HRD1. (a) Immunolocalization of HRD1 in the coronal section of the murine brain. HRD1 localization was detected by DAB immunostaining using anti-HRD1 polyclonal antibody (pAb). The magnification of the box in the left panel (×40) is part of the SNC, which is shown in the right panel (×200). The arrowheads indicate the expression of HRD1. (b) Localization of HRD1 in neurons and glia. The *green* signal (HRD1) was obtained with anti-HRD1 pAb and anti-rabbit IgG Alexa 488-conjugated secondary Ab, while the *red* signal (Pael-R) was obtained with either anti-NeuN monoclonal Ab (mAb; dentate gyrus; upper panel) or anti-GFAP mAb (CA4; lower panel) and anti-mouse IgG Alexa 546-conjugated secondary Ab. (c) Colocalization of HRD1 and tyrosine hydroxylase in the SNC of the coronal section of murine brain. HRD1 was detected by anti-HRD1 pAb (*green*); tyrosine hydroxylase was detected by antityrosine hydroxylase mAb (*red*). *Yellow* indicates the co-expression of H-RD1 in the SNC. (d) Colocalization of HRD1 and Pael-R in the endoplasmic reticulum. COS-1 cells were transiently transfected with HRD1-myc and Pael-R-FLAG. At 24 h after transfection, the cells were fixed and subjected to indirect immunofluorescence staining with anti-myc mAb and anti-FLAG pAb, or anti-calreticulin pAb. The *green* signal (HRD1) was obtained with anti-mouse IgG Alexa 488-conjugated secondary Ab and the *red* signal (Pael-R or calreticulin) with anti-rabbit IgG Alexa 594-conjugated secondary Ab. Superimposing the two colors (merge) resulted in a *yellow* signal, indicating the colocalization of the two proteins. (e) Colocalization of HRD1 and Pael-R in the endoplasmic reticulum of SH-SY5Y cells. The SH-SY5Y cells expressing Pael-R-FLAG were fixed and subjected to indirect immunofluorescence staining with anti-FLAG mAb (*red*) and anti-HRD1 pAb (*green*). The *green* signal (HRD1) was obtained with anti-rabbit IgG Alexa 488-conjugated secondary Ab and the *red* signal (Pael-R) with anti-mouse IgG Alexa 594-conjugated secondary Ab.

between Pael-R and HRD1 in native SH-SY5Y cells under endoplasmic reticulum stress. HRD1 was precipitated with Pael-R that tends to exist in an unfolded state under endoplasmic reticulum stress conditions (Fig. 2d, lane 4); this indicates that HRD1 interacts with the unfolded form of Pael-R.

HRD1 interacts with and ubiquitinates Pael-R through the proline-rich region

To investigate which HRD1 region interacts with Pael-R, a series of HRD1 mutants was prepared (Fig. 3a). HEK293 cells were transiently transfected with Pael-R-FLAG along with an empty vector (Mock), wild-type (wt)-HRD1-myc,

© 2006 The Authors
Journal Compilation © 2006 International Society for Neurochemistry,

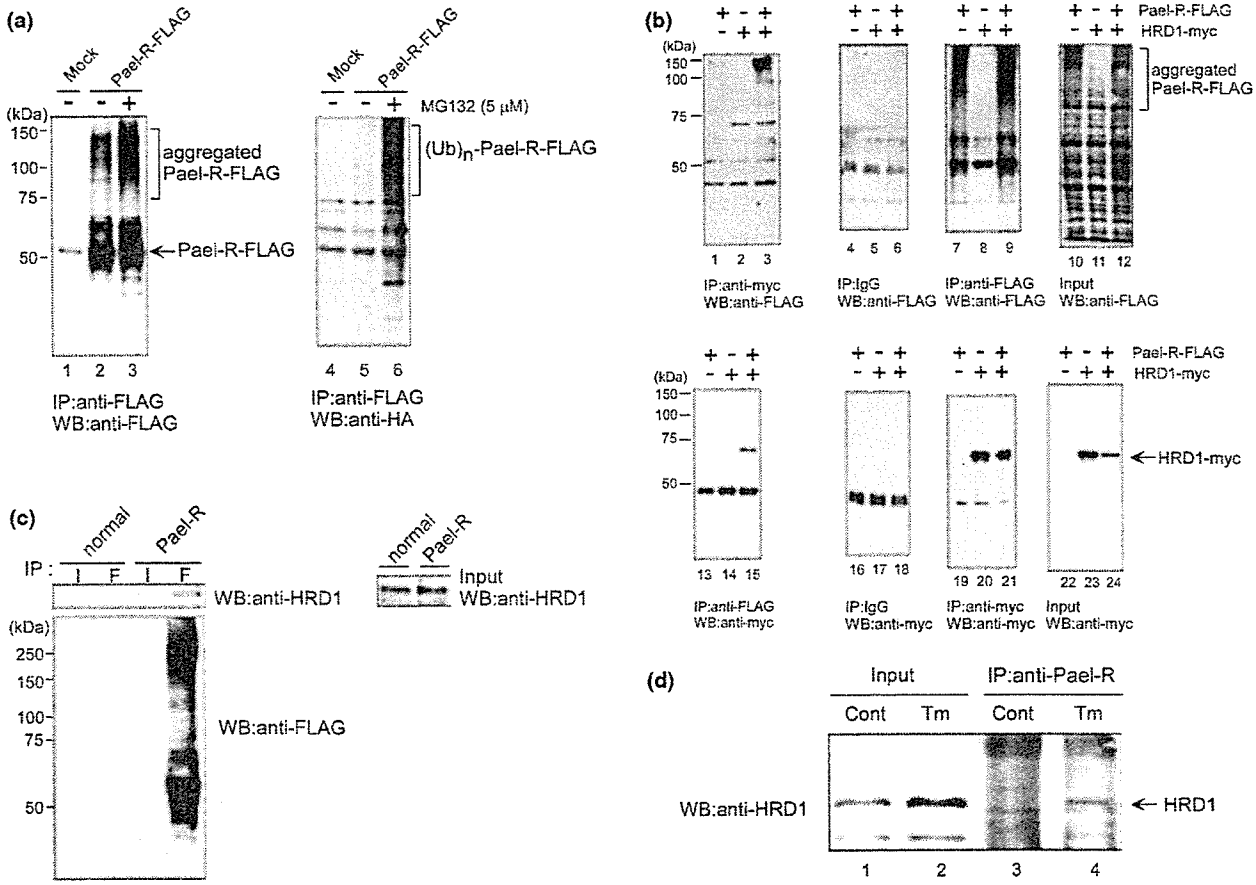

Fig. 2 Interaction of HRD1 with aggregated Pael-R. (a) Pael-R tends to exist in an aggregated form. HEK293 cells were transiently transfected with hemagglutinin-ubiquitin and an empty vector (Mock) or Pael-R-FLAG and incubated in the presence or absence of 5 μM MG132 (proteasome inhibitor). Equal amounts of proteins were immunoprecipitated with anti-FLAG mAb, and the immune complex was then analyzed by western blotting using anti-FLAG mAb (left) or anti-hemagglutinin pAb (right). (b) Interaction of Pael-R with HRD1 in HEK293 cells. HRD1 and Pael-R were coimmunoprecipitated in HEK293 cells transiently transfected with or without Pael-R-FLAG and HRD1-myc. At 48 h after transfection, the total cell lysates (Input) were analyzed by western blotting to check the expression of Pael-R and HRD1 proteins. Equal amounts of the proteins were immunoprecipitated with normal mouse IgG, anti-myc mAb, or anti-FLAG mAb. The immune complex was lysed in SDS sample buffer, resolved by SDS-PAGE, and analyzed by western blotting using anti-myc mAb or anti-FLAG mAb. (c) Endogenous HRD1 interacts with Pael-R in neuroblastoma SH-SY5Y cells stably expressing Pael-R-FLAG. The total cell lysates that stably expressed Pael-R-FLAG in neuroblastoma SH-SY5Y cells were analyzed by western blotting using anti-HRD1 pAb (Input, right panel). Equal amounts of the proteins were immunoprecipitated with normal mouse IgG (I) or anti-FLAG mAb (F), and the immune complex was then analyzed by western blotting using anti-HRD1 pAb (left panel, upper) or anti-FLAG mAb (right panel, lower). (d) Endogenous interaction of HRD1 with Pael-R in tunicamycin-treated neuroblastoma SH-SY5Y cells. The SH-SY5Y cells were either untreated (control) or treated (tunicamycin) with 2.5 μg/mL tunicamycin for 24 h. The total cell lysates (Input, lanes 1 and 2) were analyzed by western blotting to check the expression of HRD1 proteins. Equal amounts of proteins were immunoprecipitated with anti-Pael-R pAb. The immune complex was analyzed by western blotting by using anti-HRD1 pAb (IP, lanes 3 and 4; Abgent).

membrane (M)-HRD1 Δmembrane (ΔM)-HRD1-myc, or membrane-RING (MR)-HRD1-myc. Wt-HRD1 and ΔM-HRD1 were detected in immunoprecipitates with anti-FLAG, whereas (M)-HRD1 and (MR)-HRD1 were not detected (Fig. 3b, upper, lanes 3, 5), suggesting that HRD1 requires a proline-rich region for association with Pael-R. We examined whether Pael-R interacts with the proline-rich region of HRD1 *in vitro* (Fig. 4a). In an *in vitro* GST pull-down assay, RP-HRD1 bound to both the native and aggregated forms of Pael-R (Fig. 4a, upper, lane 5). Thus, HRD1 may directly interact with Pael-R through the proline-rich region.

We then evaluated whether HRD1 ubiquitinates Pael-R through its E3 activity *in vitro*. Using RP-HRD1-myc and Pael-R-FLAG generated by *in vitro* translations (Fig. 4b), we examined whether Pael-R is ubiquitylated by RP-HRD1 *in vitro*. Recombinant E2 UbcH5c was used in this assay as HRD1 is shown to be ubiquitylated by UbcH5c *in vitro* (Nadav *et al.* 2003; Kikkert *et al.* 2004). *In vitro* transcrip-

© 2006 The Authors

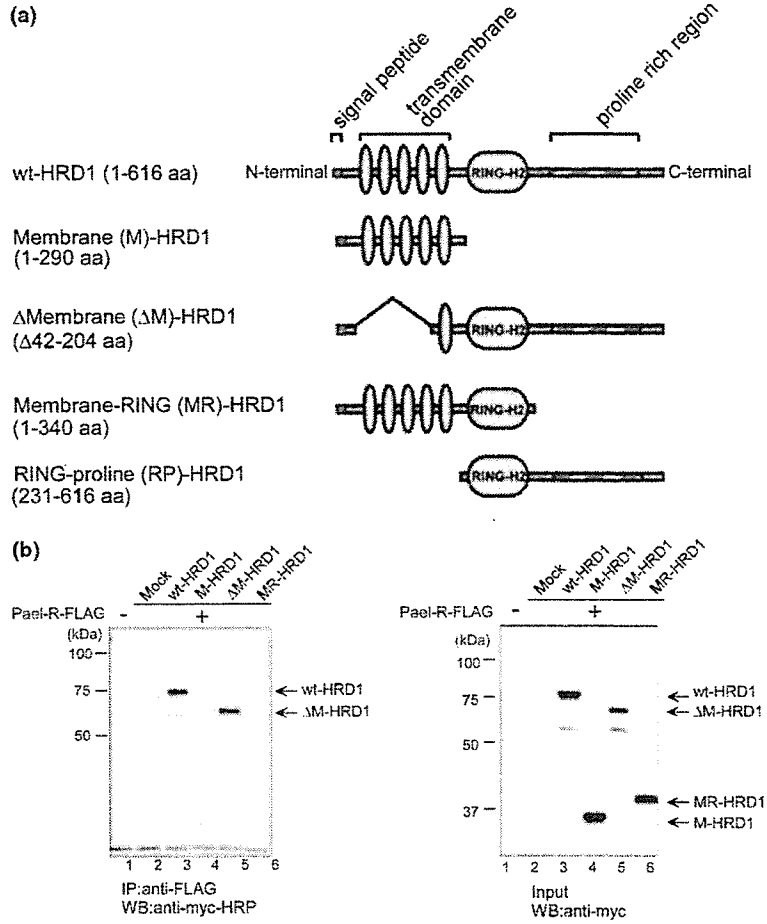

Fig. 3 Interaction of Pael-R with HRD1 and its mutants. (a) Schematic representation of the HRD1 constructs. The panel diagrammatically represents wild-type HRD1 and a variety of HRD1 mutants used to determine the Pael-R binding domain. Numbers in parentheses indicate the corresponding amino acid residues of HRD1. (b) Coimmunoprecipitation of Pael-R and a variety of HRD1 mutants. Coimmunoprecipitation was performed in HEK293 cells transiently transfected with Pael-R-FLAG and an empty vector (Mock), wild-type (wt)-HRD1-myc, membrane (M)-HRD1-myc, Δmembrane (ΔM)-HRD1-myc or membrane-RING (MR)-HRD1-myc. At 48 h after transfection, the total cell lysates (Input) were analyzed by western blotting using antimyc mAb (right). Equal amounts of the proteins were immunoprecipitated with anti-FLAG mAb, and the immune complex was then analyzed by western blotting using antimyc mAb (left).

tion/translation reaction lysates containing RP-HRD1 and Pael-R were incubated with other components including E1 (rabbit), E2 (GST-UbcH5c), and GST-ubiquitin. Pael-R-FLAG proteins were ubiquitylated only in the presence of RP-HRD1 along with all other components (Fig. 4c, lane 6), indicating that HRD1 directly interacts with and ubiquitinates Pael-R.

HRD1 degrades unfolded Pael-R

We investigated whether HRD1 accelerates Pael-R degradation via the UPS. Normal HEK293 cells and those stably expressing wt-HRD1 or M-HRD1 were transiently transfected with Pael-R-FLAG. Equal amounts of proteins were immunoprecipitated with anti-FLAG monoclonal antibody and subjected to western blotting. Pael-R and its high molecular mass broad smears were markedly decreased in wt-HRD1-expressing cells (Fig. 5a, first panel, lanes 5, 6). MG132 inhibited the decrease of Pael-R protein (Fig. 5a, first panel, lane 7), indicating that HRD1 promoted the degradation of Pael-R via the UPS. In contrast, Pael-R was not degraded by M-HRD1, which has no RING-finger domain and lacks E3 activity (Fig. 5a, first panel, lanes 8, 9). To confirm that these results were not caused by a decrease in the transfection or transcription efficiency of Pael-R, the expression level of Pael-R mRNA was examined by RT-PCR using the total RNA of the cells used in western blotting. In each clone, the expression levels of transfected Pael-R were almost equal (Fig. 5a, third panel); furthermore, another clone stably expressing wt-HRD1 degraded Pael-R (data not shown).

To immunocytochemically visualize the degradation of Pael-R by HRD1, normal HEK293 cells and those stably

© 2006 The Authors
Journal Compilation © 2006 International Society for Neurochemistry,

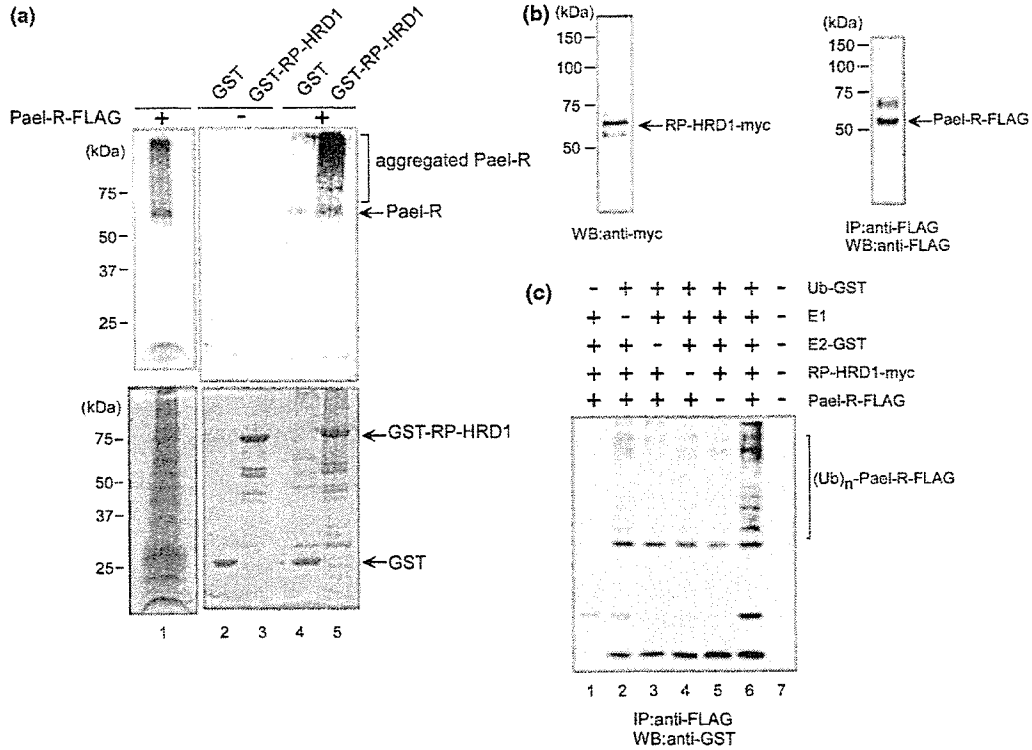

Fig. 4 HRD1 ubiquitinates Pael-R *in vitro*. (a) Coimmunoprecipitation of Pael-R with RING-proline (RP)-HRD1 *in vitro*. GST-fused RP-HRD1 or GST alone was bound to glutathione beads incubated with [^{35}S]-labeled Pael-R generated by an *in vitro* transcription/translation system. After extensive washing, the protein-bound beads were resolved by SDS-PAGE followed by Coomassie blue staining (lower), and detected by autoradiography (upper). (b) Protein products of Pael-R and RP-HRD1. Western blotting analysis of the components used for *in vitro* ubiquitylation assays. RP-HRD1-myc and Pael-R-FLAG were produced by a T_NT quick-coupled transcription/translation system. T_NT reaction lysates containing RP-HRD1 were analyzed by western blotting using anti-myc mAb (left), whereas T_NT reaction lysates containing Pael-R were immunoprecipitated with anti-FLAG mAb. The immune complex was then analyzed by western blotting using anti-FLAG mAb (right). (c) *In vitro* ubiquitylation assay. Western blotting analysis of the *in vitro* ubiquitylation reactions mediated by HRD1 with anti-GST pAb. T_NT reaction lysates containing RP-HRD1 and Pael-R were mixed with other components including E1 (rabbit), E2 (GST-UbcH5c), or GST-ubiquitin in the reaction buffer. The reaction lysates were then incubated at 30°C for 90 min, immunoprecipitated with anti-FLAG mAb, and analyzed by western blotting using anti-GST pAb.

expressing wt-HRD1 or M-HRD1 were transfected with Pael-R-FLAG and DsRED, a red fluorescent protein. The amount of Pael-R-FLAG protein decreased in cells expressing wt-HRD1-myc compared with control cells, whereas the amount of Pael-R-FLAG protein in cells expressing M-HRD1-myc and in control cells was similar (Fig. 5b, upper, *green*). The red signals (lower panels) were DsRED proteins cotransfected with Pael-R-FLAG for use as transfection controls. These results indicate that HRD1 degrades Pael-R by its E3 activity.

Next, the degradation of Pael-R by HRD1 was examined by performing a pulse-chase experiment. The levels of ^{35}S-labeled Pael-R were plotted relative to the amount present at time 0 (Fig. 5c). Following a 3 h chase, 54.4% and 52.0% of *de novo* synthesized Pael-R remained in cells transfected with Mock and M-HRD1, respectively. In contrast, Pael-R degradation in HRD1-transfected cells was accelerated such that at 3 h, 28.7% of proteins remained, indicating that HRD1 accelerates the degradation of newly synthesized Pael-R protein.

Furthermore, to investigate whether HRD1 is involved in the physiological degradation of Pael-R, we examined the effect of HRD1 suppression by siRNA on Pael-R accumulation in SH-SY5Y cells stably expressing Pael-R-FLAG. The amount of the aggregated form of Pael-R was increased by the suppression of HRD1 expression (Fig. 5d, upper, lane 2) whereas the native form was not affected markedly; thus, it is possible that endogenous HRD1 preferentially degrades aggregated Pael-R but not native Pael-R.

α-Synuclein is a component of Lewy bodies in Parkinson's disease (Trojanowski *et al.* 1998), and a 22-kD glycosylated form of α-synuclein is reported to be ubiquitylated by Parkin (Shimura *et al.* 2001), and is ubiquitylated when overexpressed in cells (Imai *et al.* 2000). Unfolded α-synuclein can be degraded by the 20S proteasome *in vitro* (Tofaris *et al.* 2001). We examined whether α-synuclein, like Pael-R, is a

© 2006 The Authors

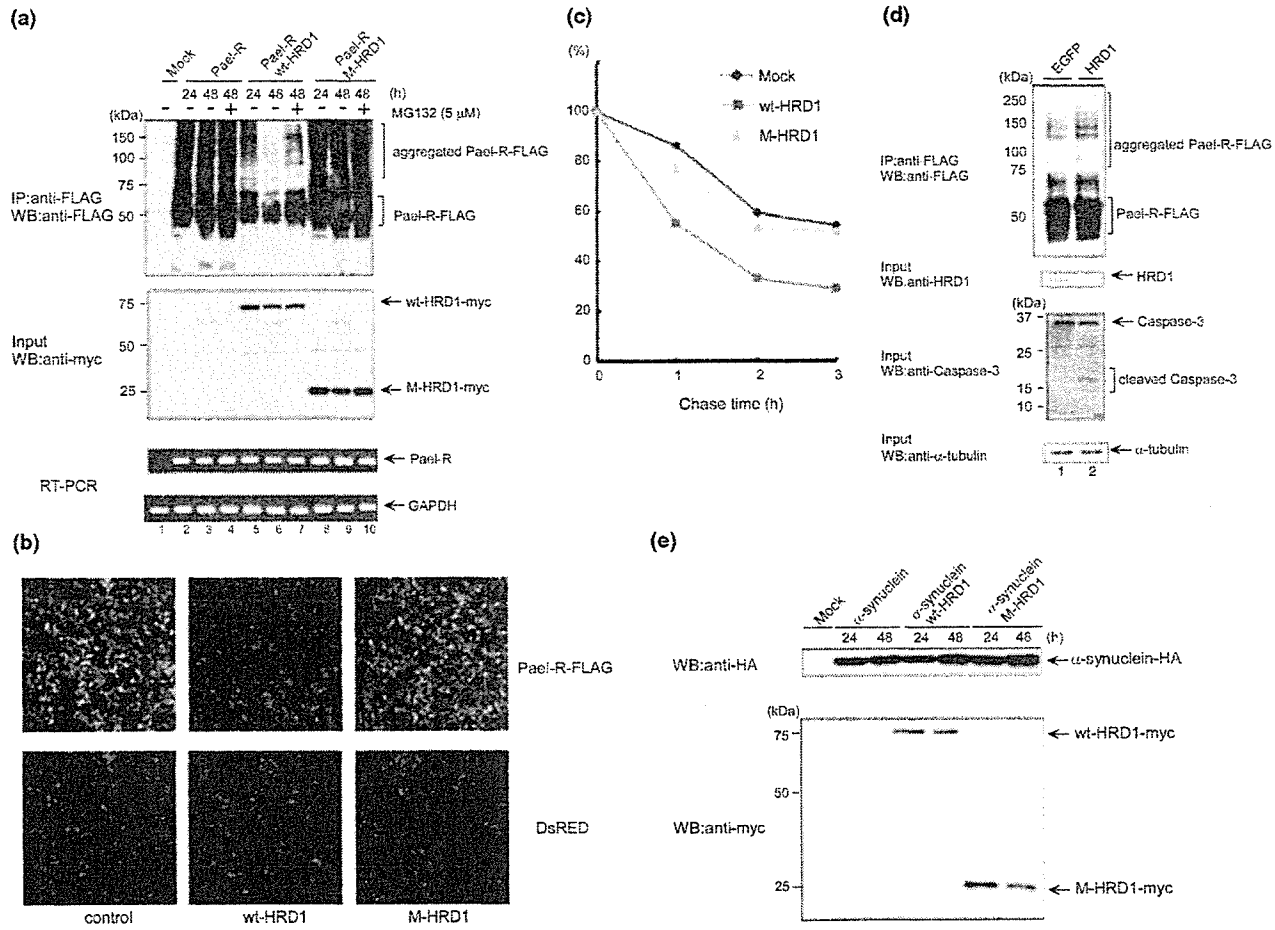

Fig. 5 Degradation of Pael-R by HRD1. (a) HEK293 cells stably expressing wt-HRD1 or M-HRD1 were transiently transfected with Pael-R-FLAG and incubated for the indicated periods in the presence or absence of 5 μM MG132, which was added 12 h before cell harvest. The total cell lysates (Input) were analyzed by western blotting using anti-myc mAb (middle). Equal amounts of the proteins were immunoprecipitated with anti-FLAG mAb, and the immune complex was then analyzed by western blotting using anti-FLAG mAb (upper). The total RNA of the cells used in western blotting was prepared and subjected to RT-PCR (lower). (b) HEK293 cells stably expressing wt-HRD1 or M-HRD1 were transiently transfected with Pael-R-FLAG and DsRED (red fluorescent protein). At 36 h after transfection, the cells were fixed and subjected to indirect immunofluorescence staining with anti-FLAG mAb (upper). The *green* signal (Pael-R) was obtained with anti-mouse IgG Alexa 488-conjugated secondary Ab while the *red* signal (lower) shows DsRED proteins used as a transfection control. (c) Pulse-chase assay. Neuro2a cells were transiently transfected with Pael-R-FLAG and an empty vector (Mock), wt-HRD1, or M-HRD1. At 36 h after transfection, cells were pulse-labeled with [^{35}S]-methionine/cysteine and chased for the indicated periods. Equal amounts of [^{35}S]-labeled Pael-R and M-HRD1 were immunoprecipitated with anti-FLAG mAb; the immune complex was then lysed in SDS sample buffer, resolved by SDS-PAGE, detected by autoradiography, and quantified by phosphorimaging. The levels of [^{35}S]-labeled Pael-R are plotted relative to the amount present at time 0. (d) Induction of aggregated Pael-R accumulation and caspase activation by inhibition of HRD1 expression. SH-SY5Y cells stably expressing Pael-R-FLAG were transiently transfected with the siRNA of enhanced green fluorescent protein (EGFP, control) or HRD1, and incubated for 72 h. The total cell lysates were analyzed by western blotting using anti-HRD1 pAb (2nd panel), anti-caspase-3 pAb (3rd panel), and anti-α-tubulin mAb (5th panel). Equal amounts of the proteins were immunoprecipitated with anti-FLAG mAb, and the immune complex was then analyzed by western blotting using anti-FLAG mAb (1st panel). (e) HRD1 did not degrade α-synuclein. HEK293 cells stably expressing wt-HRD1 or M-HRD1 were transiently transfected with α-synuclein-hemagglutinin and incubated for the indicated periods. The total cell lysates were analyzed by western blotting using anti-hemagglutinin pAb (upper) or anti-myc mAb (lower).

substrate of HRD1. Normal HEK293 cells and those stably expressing wt- or M-HRD1 were transiently transfected with α-synuclein-hemagglutinin. The protein levels of α-synuclein were not changed by HRD1 (Fig. 5e, upper), indicating that α-synuclein is not a substrate of HRD1.

HRD1 suppresses Pael-R-induced cell death

The accumulation of Pael-R causes endoplasmic reticulum stress and subsequent cell death. We investigated whether HRD1 suppresses Pael-R-induced cell death. Normal HEK293 cells and those stably expressing wt- or M-HRD1

© 2006 The Authors
Journal Compilation © 2006 International Society for Neurochemistry,

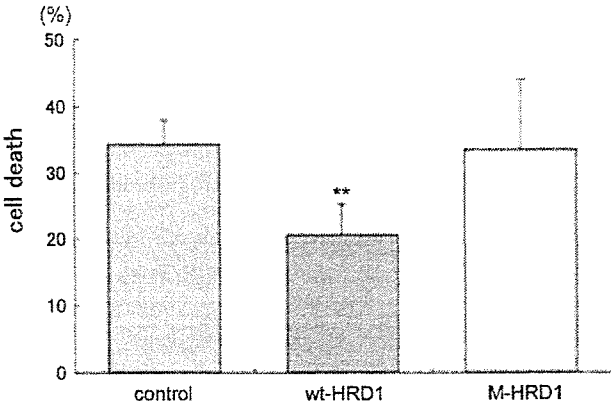

Fig. 6 HRD1 protects against Pael-R-induced cell death. HEK293 cells (control) and HEK 293 cells stably expressing wt-HRD1 or M-HRD1 were transiently transfected with a control vector (Mock) or Pael-R-FLAG and incubated for 24 h. The cells were washed with PBS and then stained with crystal violet (0.1%) for 20 min, and the wells were washed with water and air-dried. The dye was eluted with water containing 0.5% SDS for 20 min, and the optical density at 590 nm was measured. The percentage of cell death was calculated as follows: 100 – [(OD for assay/OD for control well) × 100]. The results obtained from each cell transfected with Pael-R-FLAG were compared with those obtained from cells transfected with Mock. The results are expressed as the means ± SD (three independent experiments in duplicate). Statistical analysis was performed with Student's *t*-test (**$p < 0.01$, vs. normal).

were transiently transfected with a control vector (Mock) or Pael-R-FLAG and incubated for 24 h. The cell death of HEK293 was compared with that of cells transfected with the control vector. The crystal violet assay showed that wt-HRD1-expressing cells were more resistant to Pael-R overexpression than control and M-HRD1 cells (control, 34.3%; wt-HRD1, 20.8%; M-HRD1, 33.4%) (Fig. 6). Furthermore, we found that the accumulation of aggregated Pael-R induced by the repression of HRD1 in SH-SY5Y cells that stably expressed Pael-R-FLAG promoted a decrease in pro-caspase-3 and an increase in cleaved caspase-3 (Fig. 5d, third panel, lane 2), which indicates the activation of caspase-3 and subsequent apoptosis. These results indicate that HRD1 suppresses apoptosis induced by Pael-R accumulation.

Involvement of HRD1 in the degradation of Pael-R induced by ATF6

We found that ATF6 induced the expression of HRD1 (Kaneko *et al.* 2002; unpublished data). As ATF6-mediated UPR possibly induces a number of ERAD genes, we speculated that the degradation of Pael-R is promoted by ATF6. HEK293 cells were transiently transfected with Pael-R-FLAG and either an empty vector (Mock) or hemagglutinin-ATF6 (1–373; cytoplasmic domain worked as a transcription factor), and incubated for 48 h in the presence or absence of MG132. The amount of both native and aggregated Pael-R decreased in cells expressing ATF6

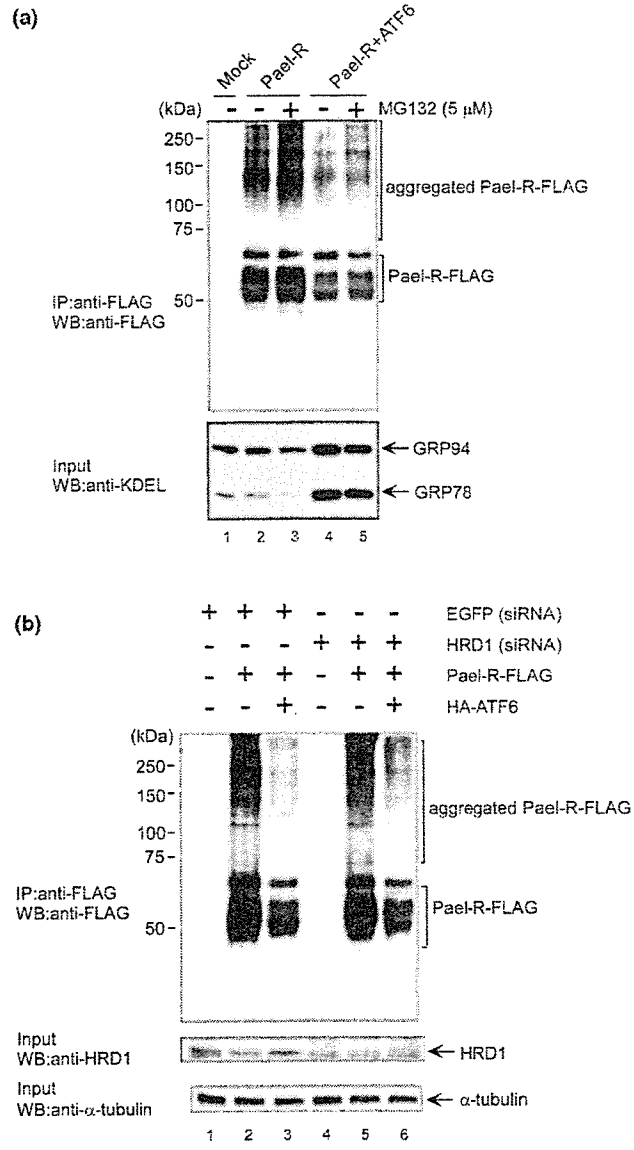

Fig. 7 Degradation of Pael-R promoted by ATF6. (a) HEK293 cells were transiently transfected with an empty vector (Mock) or Pael-R-FLAG with or without hemagglutinin-ATF6 (cleaved form); they were incubated for 48 h in the presence or absence of 5 μM MG132 (12 h incubation). The total cell lysates (Input) were analyzed by western blotting using anti-KDEL mAb (lower). Equal amounts of the proteins were immunoprecipitated with anti-FLAG mAb, and then analyzed by western blotting using anti-FLAG mAb (upper). (b) Involvement of HRD1 in ATF6-mediated Pael-R degradation. HEK293 cells were transiently transfected with Pael-R-FLAG and hemagglutinin-ATF6 (cleaved form) and siRNA of EGFP (control) or HRD1 and incubated for 30 h. The total cell lysates (Input) were analyzed by western blotting using anti-HRD1 pAb (middle) or anti-α-tubulin mAb (lower). Equal amounts of the proteins were immunoprecipitated with anti-FLAG mAb, and the immune complex was then analyzed by western blotting using anti-FLAG mAb (upper).

© 2006 The Authors

(Fig. 7a, upper, lane 4); moreover, MG132 inhibited the decrease in Pael-R protein by ATF6 overexpression (Fig. 7a, upper, lane 5). The increased expression of glucose-regulated proteins GRP78 and GRP94 indicates the induction of UPR by ATF6 (Fig. 7a, lower, lanes 4, 5). These results indicate that the up-regulation of UPR by ATF6 leads to the degradation of Pael-R proteins via the UPS; however, it is not known which proteins induced by ATF6 are involved in this degradation.

To determine whether HRD1 is involved in the degradation of Pael-R induced by UPR up-regulation, we investigated the effect of HRD1 suppression by siRNA on degradation. HEK293 cells were transiently transfected with Pael-R-FLAG, hemagglutinin-ATF6, and either green fluorescent protein (GFP) (siRNA) or HRD1 (siRNA). ATF6 induced HRD1 expression (Fig. 7B, lower, lane 3), whereas HRD1 repression partially suppressed the ATF6-induced decrease in the number of Pael-R aggregates, but not the amount of the native form (Fig. 7b, upper, lane 6), suggesting that UPR-induced HRD1 preferentially promotes the degradation of unfolded Pael-R.

Discussion

In this report, we found that HRD1 was expressed in the dopaminergic neurons of the SNC, colocalized with Pael-R in the endoplasmic reticulum, and directly interacted with Pael-R at the proline-rich region of HRD1. We showed that HRD1 promoted the ubiquitylation and degradation of Pael-R; additionally, the activation of UPR by ATF6 induced Pael-R degradation, which partially depends on HRD1.

First, we found that HRD1 was locally expressed in SNC neurons, including dopaminergic neurons, of the murine brain. Pael-R is reportedly expressed in SNC neurons, implying that HRD1 and Pael-R are colocalized in dopaminergic neurons in the SNC. Parkin, an E3, is up-regulated in response to endoplasmic reticulum stress and protects cells via ERAD from endoplasmic reticulum stress-induced apoptosis (Imai *et al.* 2000). Pael-R accumulates in the brains of AR-JP patients and induces endoplasmic reticulum stress, possibly because of Parkin mutation (Imai *et al.* 2001). Furthermore, it has been reported that Pael-R overexpression causes the selective degeneration of dopaminergic neurons in *Drosophila* and that the coexpression of human Parkin suppresses Pael-R toxicity by degrading Pael-R. It has also been reported that interference in endogenous *Drosophila* Parkin functions enhances Pael-R toxicity (Yang *et al.* 2003). On the other hand, we previously reported that human HRD1 is up-regulated in response to endoplasmic reticulum stress. It possesses E3 activity and protects against endoplasmic reticulum stress-induced cell death (Kaneko *et al.* 2002), suggesting that HRD1 can degrade protein substrates accumulated during endoplasmic reticulum stress. There is, however, little information regarding these substrates, with the exception of CD-3α and TCR-α, and HMG-CoA reductase (Kikkert *et al.* 2004). We showed that HRD1 was colocalized in the endoplasmic reticulum with Pael-R and they interacted at endogenous levels as well as overexpression levels. We therefore hypothesized that HRD1, like Parkin, may degrade Pael-R and suppress cell death caused by Pael-R accumulation.

We found that endogenous HRD1 interacted with not only overexpressed Pael-R but also endogenous Pael-R under endoplasmic reticulum stress conditions. Pael-R tends to exist in an unfolded state when it is overexpressed or when subjected to endoplasmic reticulum stress; therefore, it is likely that HRD1 preferentially interacts with the unfolded form of Pael-R but not with the normally folded form. Therefore, it can be speculated that unfolded Pael-R is recognized by acceptors of terminally misfolded glycoproteins, such as endoplasmic reticulum degradation-enhancing alpha-mannosidase-like protein (EDEM), and is destined to be eliminated from the endoplasmic reticulum (Molinari *et al.* 2003; Oda *et al.* 2003); HRD1 then binds to Pael-R passing through the translocon in the endoplasmic reticulum membrane by its proline-rich region and ubiquitinates the unfolded form of Pael-R. If this is true, it is unlikely that HRD1 directly associates with and ubiquitinates native Pael-R on the endoplasmic reticulum membrane without mediation of the translocon.

On the other hand, we showed that the high molecular mass broad smears of Pael-R mostly comprised not ubiquitylated forms, but possibly glycosylated or aggregated forms, as previously reported (Imai *et al.* 2001). The inhibition of HRD1 expression by siRNA induced the accumulation of smears and the activation of caspase-3. Therefore, it is likely that HRD1 preferentially ubiquitinates and degrades unfolded Pael-R to prevent the accumulation of aggregated Pael-R that leads to endoplasmic reticulum stress-induced apoptosis.

We further showed that HRD1 interacted with Pael-R at its proline-rich region and ubiquitylated Pael-R *in vitro*, indicating direct interaction between the proline-rich region of HRD1 and Pael-R. Yeast Hrd1p has no proline-rich region, whereas human HRD1 contains a proline-rich region similar to that seen in the Cbl family of ubiquitin ligases (Fujita *et al.* 2002). It has been reported that the proline-rich region is essential for protein–protein interaction and that the RING-finger and proline-rich regions are sufficient for the binding and ubiquitylation of substrates (Fang *et al.* 2001). Therefore, human HRD1 appears to interact with substrates at the proline-rich region and ubiquitinates the substrates at the RING-finger domain. On the other hand, Hrd1p degrades Hmg2p, one of the yeast isozymes of HMG-CoA reductase, despite the lack of a proline-rich region (Gardner *et al.* 2000). Thus, we propose that in the course of evolution, human HRD1 acquired a proline-rich region to interact with and ubiquitinate a variety of substrates; whether other

© 2006 The Authors
Journal Compilation © 2006 International Society for Neurochemistry,

substrates are bound to the proline-rich region remains to be determined.

We investigated whether α-synuclein is a substrate of HRD1. An α-synuclein mutant (Ala53Thr or Ala30Pro) has been reported in the brain of Parkinson's disease patients, promoting protofibril formation relative to wild-type α-synuclein (Conway *et al.* 2000). Parkin ubiquitinates the *O*-glycosylated form (αSp22) (Shimura *et al.* 2001) and suppresses the toxicity of normal or pathogenic alpha-synuclein (Petrucelli *et al.* 2002; Yang *et al.* 2003; Lo Bianco *et al.* 2004; Haywood and Staveley 2004). HRD1 did not degrade wild-type α-synuclein, probably due to the different localization or binding ability of HRD1 and α-synuclein; however, whether HRD1 degrades α-synuclein mutants or the *O*-glycosylated form remains to be clarified. On the other hand, Hrd3p, another UPR-inducible ERAD protein, has been reported to interact with Hrd1p and mediate the regulation of Hrd1p stability and activity in yeast (Gardner *et al.* 2000). We have identified SEL1 as a candidate human homolog of Hrd3p and have found that SEL1 interacted with human HRD1 (data not shown). We have further found that HRD1 did not degrade SEL1 despite this interaction; rather, the amount of SEL1 increased in the presence of HRD1 (data not shown). Based on these observations, we speculate that HRD1 specifically increases the degradation of proteins.

When unfolded proteins accumulate in the endoplasmic reticulum, the UPR is activated by ATF6 and IRE1, resulting in the induction of several endoplasmic reticulum chaperones and ERAD components (Travers *et al.* 2000; Lee *et al.* 2003). Therefore, we hypothesized that ATF6 promotes the degradation of Pael-R by inducing UPR genes including HRD1, although ATF6 can induce a variety of genes in addition to HRD1. Interestingly, ATF6 induced the degradation of both aggregated and unaggregated Pael-R, whereas the suppression of ATF6-induced HRD1 expression by siRNA caused an increase in the aggregated form. Thus, it is likely that endogenous HRD1 preferentially recognizes and degrades the unfolded forms of Pael-R. Based on these results, we propose that after the accumulation of unfolded Pael-R due to stress or Parkin mutation, ATF6 and/or IRE1-XBP1 pathways are activated and induce UPR genes including HRD1; this promotes the folding or degradation of unfolded Pael-R to prevent unfolded Pael-R-induced cell death (Fig. 8).

It has been reported that Parkin knockout mice exhibit little change in movement ability or the neurons of the substantia nigra (Itier *et al.* 2003; Goldberg *et al.* 2003; von Coelln *et al.* 2004; Perez and Palmiter 2005). We therefore speculate that HRD1 degrades Pael-R and possibly other proteins to balance the unfolded protein accumulation caused by Parkin gene mutation; nonetheless, it is possible that other unknown E3s participate in this degradation in the absence of Parkin, although the reason behind the loss of dopaminergic neurons in AR-JP patients but not in Parkin knockout mice remains unknown despite the similarity in the functional loss of Parkin. On the other hand, it is likely that HRD1 ubiquitinates not only Pael-R but also other substrates related to conformational diseases caused by the accumulation of unfolded proteins as HRD1 can suppress global endoplasmic reticulum stress induced by various chemical reagents.

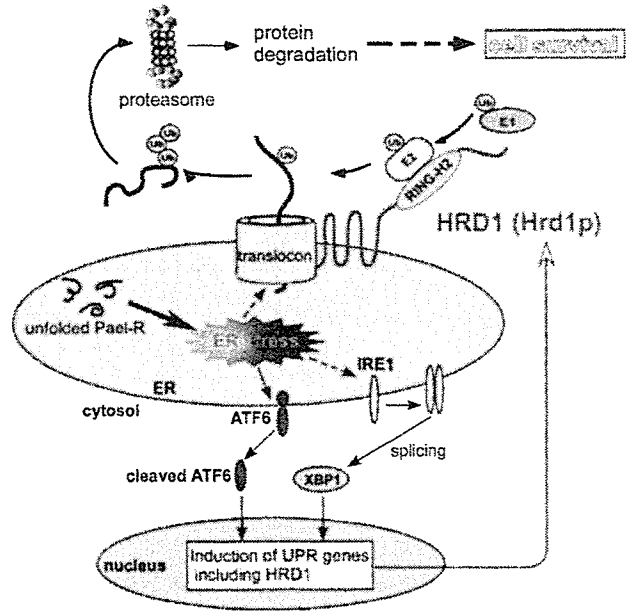

Fig. 8 A hypothetical model demonstrating how HRD1 participates in the degradation of unfolded Pael-R. When unfolded Pael-R is accumulated in the endoplasmic reticulum, ATF6 and IRE1-XBP1 pathways are activated, and UPR genes including HRD1 are then induced. HRD1 degrades unfolded Pael-R and suppresses Pael-R-induced cell death.

Acknowledgements

We are grateful to Dr. Yuzuru Imai for his helpful discussions. We thank Otsuka GEN Research Institute for providing the HRD1 antibody. We also thank Dr. Takahiro Taira and Mr. Takanori Tabata for their helpful discussions. We thank Mr. T. Itou, Mitsubishi Chemical Safety Institute, LTD. for pertinent advises on immunohistochemical study. This study was supported by Grants-in-Aid for Scientific Research from the Ministry of Education, Culture, Sports, Science and Technology, Japan.

References

Amano T., Yamasaki S., Yagishita N. *et al.* (2003) Synoviolin/Hrd1, an E3 ubiquitin ligase, as a novel pathogenic factor for arthropathy. *Genes Dev.* **17**, 2436–2449.

Conway K. A., Lee S. J., Rochet J. C., Ding T. T., Williamson R. E. and Lansbury P. T. Jr (2000) Acceleration of oligomerization, not fibrillization, is a shared property of both alpha-synuclein muta-

© 2006 The Authors

tions linked to early-onset Parkinson's disease: implications for pathogenesis and therapy. *Proc. Natl Acad. Sci. U S A* **97**, 571–576.

Cox J. S., Shamu C. E. and Walter P. (1993) Transcriptional induction of genes encoding endoplasmic reticulum resident proteins requires a transmembrane protein kinase. *Cell* **73**, 1197–1206.

Deak P. M. and Wolf D. H. (2001) Membrane topology and function of Der3/Hrd1p as a ubiquitin-protein ligase (E3) involved in endoplasmic reticulum degradation. *J. Biol. Chem.* **276**, 10 663–10 669.

Fang D., Wang H. Y., Fang N., Altman Y., Elly C. and Liu Y. C. (2001) Cbl-b, a RING-type E3 ubiquitin ligase, targets phosphatidylinositol 3-kinase for ubiquitination in T cells. *J. Biol. Chem.* **276**, 4872–4878.

Friedlander R., Jarosch E., Urban J., Volkwein C. and Sommer T. (2000) A regulatory link between ER-associated protein degradation and the unfolded protein response. *Nat. Cell Biol.* **2**, 379–384.

Fujita Y., Krause G., Scheffner M., Zechner D., Leddy H. E., Behrens J., Sommer T. and Birchmeier W. (2002) Hakai, a c-Cbl-like protein, ubiquitinates and induces endocytosis of the E-cadherin complex. *Nat. Cell Biol.* **4**, 222–231.

Gardner R. G., Swarbrick G. M., Bays N. W., Cronin S. R., Wilhovsky S., Seelig L., Kim C. and Hampton R. Y. (2000) Endoplasmic reticulum degradation requires lumen to cytosol signaling. Transmembrane control of Hrd1p by Hrd3p. *J. Cell Biol.* **151**, 69–82.

Gardner R. G., Shearer A. G. and Hampton R. Y. (2001) In vivo action of the HRD ubiquitin ligase complex: mechanisms of endoplasmic reticulum quality control and sterol regulation. *Mol. Cell Biol.* **21**, 4276–4291.

Goldberg M. S., Fleming S. M., Palacino J. J. *et al.* (2003) Parkin-deficient mice exhibit nigrostriatal deficits but not loss of dopaminergic neurons. *J. Biol. Chem.* **278**, 43 628–43 635.

Haywood A. F. and Staveley B. E. (2004) Parkin counteracts symptoms in a Drosophila model of Parkinson's disease. *BMC Neurosci.* **5**, 14.

Haze K., Yoshida H., Yanagi H., Yura T. and Mori K. (1999) Mammalian transcription factor ATF6 is synthesized as a transmembrane protein and activated by proteolysis in response to endoplasmic reticulum stress. *Mol. Biol. Cell* **10**, 3787–3799.

Hershko A. and Ciechanover A. (1998) The ubiquitin system. *Annu. Rev. Biochem.* **67**, 425–479.

Imai Y., Soda M. and Takahashi R. (2000) Parkin suppresses unfolded protein stress-induced cell death through its E3 ubiquitin-protein ligase activity. *J. Biol. Chem.* **275**, 35 661–35 664.

Imai Y., Soda M., Inoue H., Hattori N., Mizuno Y. and Takahashi R. (2001) An unfolded putative transmembrane polypeptide, which can lead to endoplasmic reticulum stress, is a substrate of Parkin. *Cell* **105**, 891–902.

Itier J. M., Ibanez P., Mena M. A. *et al.* (2003) Parkin gene inactivation alters behaviour and dopamine neurotransmission in the mouse. *Hum. Mol. Genet.* **12**, 2277–2291.

Kaneko M., Ishiguro M., Niinuma Y., Uesugi M. and Nomura Y. (2002) Human HRD1 protects against ER stress-induced apoptosis through ER-associated degradation. *FEBS Lett.* **532**, 147–152.

Kaufman R. J. (1999) Stress signaling from the lumen of the endoplasmic reticulum: coordination of gene transcriptional and translational controls. *Genes Dev.* **13**, 1211–1233.

Kaufman R. J., Scheuner D., Schroder M., Shen X., Lee K., Liu C. Y. and Arnold S. M. (2002) The unfolded protein response in nutrient sensing and differentiation. *Nat. Rev. Mol. Cell Biol.* **3**, 411–421.

Kikkert M., Doolman R., Dai M., Avner R., Hassink G., van Voorden S., Thanedar S., Roitelman J., Chau V. and Wiertz E. (2004) Human HRD1 is an E3 ubiquitin ligase involved in degradation of proteins from the endoplasmic reticulum. *J. Biol. Chem.* **279**, 3525–3534.

Kitada T., Asakawa S., Hattori N., Matsumine H., Yamamura Y., Minoshima S., Yokochi M., Mizuno Y. and Shimizu N. (1998) Mutations in the parkin gene cause autosomal recessive juvenile parkinsonism. *Nature* **392**, 605–608.

Lee A. H., Iwakoshi N. N. and Glimcher L. H. (2003) XBP-1 regulates a subset of endoplasmic reticulum resident chaperone genes in the unfolded protein response. *Mol. Cell. Biol.* **23**, 7448–7459.

Lo Bianco C., Schneider B. L., Bauer M., Sajadi A., Brice A., Iwatsubo T. and Aebischer P. (2004) Lentiviral vector delivery of parkin prevents dopaminergic degeneration in an alpha-synuclein rat model of Parkinson's disease. *Proc. Natl Acad. Sci. U S A* **101**, 17 510–17 515.

Mizuno Y., Hattori N. and Matsumine H. (1998) Neurochemical and neurogenetic correlates of Parkinson's disease. *J. Neurochem.* **71**, 893–902.

Molinari M., Calanca V., Galli C., Lucca P. and Paganetti P. (2003) Role of EDEM in the release of misfolded glycoproteins from the calnexin cycle. *Science* **299**, 1397–1400.

Murakami T., Shoji M., Imai Y., Inoue H., Kawarabayashi T., Matsubara E., Harigaya Y., Sasaki A., Takahashi R. and Abe K. (2004) Pael-R. is accumulated in Lewy bodies of Parkinson's disease. *Ann. Neurol.* **55**, 439–442.

Nadav E., Shmueli A., Barr H., Gonen H., Ciechanover A. and Reiss Y. (2003) A novel mammalian endoplasmic reticulum ubiquitin ligase homologous to the yeast Hrd1. *Biochem. Biophys. Res. Commun.* **303**, 91–97.

Nagase T., Nakayama M., Nakajima D., Kikuno R. and Ohara O. (2001) Prediction of the coding sequences of unidentified human genes. XX. The complete sequences of 100 new cDNA clones from brain which code for large proteins in vitro. *DNA Res.* **8**, 85–95.

Oda Y., Hosokawa N., Wada I. and Nagata K. (2003) EDEM as an acceptor of terminally misfolded glycoproteins released from calnexin. *Science* **299**, 1394–1397.

Palacino J. J., Sagi D., Goldberg M. S., Krauss S., Motz C., Wacker M., Klose J. and Shen J. (2004) Mitochondrial dysfunction and oxidative damage in parkin-deficient mice. *J. Biol. Chem.* **279**, 18 614–18 622.

Perez F. A. and Palmiter R. D. (2005) Parkin-deficient mice are not a robust model of parkinsonism. *Proc. Natl Acad. Sci. U S A.* **102**, 2174–2179.

Periquet M., Corti O., Jacquier S. and Brice A. (2005) Proteomic analysis of parkin knockout mice: alterations in energy metabolism, protein handling and synaptic function. *J. Neurochem.* **95**, 1259–1276.

Petrucelli L., O'Farrell C., Lockhart P. J., Baptista M., Kehoe K., Vink L., Choi P., Wolozin B., Farrer M., Hardy J. and Cookson M. R. (2002) Parkin protects against the toxicity associated with mutant alpha-synuclein: proteasome dysfunction selectively affects catecholaminergic neurons. *Neuron.* **36**, 1007–1019.

Plemper R. K., Bordallo J., Deak P. M., Taxis C., Hitt R. and Wolf D. H. (1999) Genetic interactions of Hrd3p and Der3p/Hrd1p with Sec61p suggest a retro-translocation complex mediating protein transport for ER degradation. *J. Cell Sci.* **112**, 4123–4134.

Shen J., Chen X., Hendershot L. and Prywes R. (2002) ER stress regulation of ATF6 localization by dissociation of BiP/GRP78 binding and unmasking of Golgi localization signals. *Dev. Cell* **3**, 99–111.

Shimura H., Schlossmacher M. G., Hattori N., Frosch M. P., Trockenbacher A., Schneider R., Mizuno Y., Kosik K. S. and Selkoe D. J. (2001) Ubiquitination of a new form of alpha-synuclein by parkin from human brain: implications for Parkinson's disease. *Science* **293**, 263–269.

© 2006 The Authors
Journal Compilation © 2006 International Society for Neurochemistry,

Sidrauski C. and Walter P. (1997) The transmembrane kinase Ire1p is a site-specific endonuclease that initiates mRNA splicing in the unfolded protein response. *Cell* **90**, 1031–1039.

Tofaris G. K., Layfield R. and Spillantini M. G. (2001) Alpha-synuclein metabolism and aggregation is linked to ubiquitin-independent degradation by the proteasome. *FEBS Lett.* **509**, 22–26.

Travers K. J., Patil C. K., Wodicka L., Lockhart D. J., Weissman J. S. and Walter P. (2000) Functional and genomic analyses reveal an essential coordination between the unfolded protein response and ER-associated degradation. *Cell* **101**, 249–258.

Trojanowski J. Q., Goedert M., Iwatsubo T. and Lee V. M. (1998) Fatal attractions: abnormal protein aggregation and neuron death in Parkinson's disease and Lewy body dementia. *Cell Death Differ.* **5**, 832–837.

Von Coelln R., Thomas B., Savitt J. M., Lim K. L., Sasaki M., Hess E. J., Dawson V. L. and Dawson T. M. (2004) Loss of locus coeruleus neurons and reduced startle in parkin null mice. *Proc. Natl Acad. Sci. U S A* **101**, 10 744–10 749.

Yang Y., Nishimura I., Imai Y., Takahashi R. and Lu B. (2003) Parkin suppresses dopaminergic neuron-selective neurotoxicity induced by Pael-R. in Drosophila. *Neuron* **37**, 911–924.

Ye J., Rawson R. B., Komuro R., Chen X., Dave U. P., Prywes R., Brown M. S. and Goldstein J. L. (2000) ER stress induces cleavage of membrane-bound ATF6 by the same proteases that process SREBPs. *Mol. Cell* **6**, 1355–1364.

Yoshida H., Matsui T., Yamamoto A., Okada T. and Mori K. (2001) XBP1 mRNA is induced by ATF6 and spliced by IRE1 in response to ER stress to produce a highly active transcription factor. *Cell* **107**, 881–891.

Zheng N., Wang P., Jeffrey P. D. and Pavletich N. P. (2000) Structure of a c-Cbl-UbcH7 complex: RING domain function in ubiquitin-protein ligases. *Cell* **102**, 533–539.

© 2006 The Authors
Journal Compilation © 2006 International Society for Neurochemistry,

Matrix Metalloproteinase-2 Plays a Critical Role in the Pathogenesis of White Matter Lesions After Chronic Cerebral Hypoperfusion in Rodents

Kayoko Nakaji, MD; Masafumi Ihara, MD; Chiaki Takahashi, MD; Shigeyoshi Itohara, PhD; Makoto Noda, PhD; Ryosuke Takahashi, MD; Hidekazu Tomimoto, MD

Background and Purpose—Cerebrovascular white matter (WM) lesions contribute to cognitive impairment and motor dysfunction in the elderly. A disruption of the blood–brain barrier (BBB) is believed to be a critical early event leading to these WM lesions. Previous studies have suggested the involvement of matrix metalloproteinase-2 (MMP-2) in BBB disruptions and the upregulation of MMP-2 after chronic cerebral hypoperfusion in a rat model. In the present study, we asked whether MMP-2 is involved in the BBB disruption and the subsequent WM lesions after chronic cerebral hypoperfusion.

Methods—We compared the severity of white matter lesions in rats after chronic cerebral hypoperfusion with or without an MMP inhibitor. Then, we also induced the chronic cerebral hypoperfusion in wild-type and MMP-2-null mice.

Results—In the rats treated with a relatively selective MMP-2 inhibitor, AG3340, the WM lesions after chronic cerebral hypoperfusion were significantly less severe, and the number of activated astroglia and microglia were also significantly lower as compared with the vehicle-treated rats. Gene knockout of MMP-2 also reduced the severity of the WM lesions and the number of activated astroglia and microglia in a mice system. In both rodents, the disruption of BBB function, as assessed by IgM staining and the Evans blue extravasation test, was less severe when MMP-2 activity was attenuated.

Conclusions—These findings indicate that MMP-2 plays a critical role in the BBB disruption, glial cell activation, and WM lesions after chronic cerebral hypoperfusion and suggest the potential value of MMP-2 inhibitors as a therapeutic tool in cerebrovascular WM lesions. **(*Stroke*. 2006;37:2816-2823.)**

Key Words: blood–brain barrier ■ chronic cerebral hypoperfusion ■ MMP inhibitor ■ MMP-2 ■ white matter lesion

Cerebrovascular white matter (WM) lesions, a neurodegenerative condition characterized by hyperintense signals on magnetic resonance images, are frequently associated with aging and cerebrovascular disease and are responsible for the cognitive decline of the elderly. Chronic cerebral ischemia is likely to cause these WM lesions, because cerebral blood flow is decreased in these patients.[1] Indeed, similar WM lesions can be induced in rats and mice after chronic cerebral hypoperfusion, the experimental conditions mimicking chronic cerebral ischemia in humans.[2,3]

Matrix metalloproteinases (MMPs) are a family of endopeptidases that can degrade most of the major constituents of the extracellular matrix.[4] MMP-2 and MMP-9 represent a subgroup of the MMP family and degrade several extracellular matrix components, including type IV collagen, fibronectin, and gelatin. Deregulated MMPs have been implicated in the tissue destruction associated with cancer, arthritis, and multiple sclerosis.[4] MMPs may also play a role in neurologic disorders. For instance, MMP-9 is increased in human brains after stroke,[5] and MMP-2 and MMP-3 are increased in cerebrovascular WM lesions from patients with vascular dementia.[6] A reduction in the basement membrane components, including type IV collagen, is associated with the blood–brain barrier (BBB) disruption during cerebral ischemia.[7] In our previous study on chronic cerebral hypoperfusion, the BBB disruption was accompanied by an upregulation of MMP-2 but not MMP-9,[8] suggesting the specific involvement of MMP-2 in the WM lesions. We hypothesize that the MMP-2 upregulation after chronic cerebral hypoperfusion correlates with BBB damage, which leads to glial activation and subsequent WM lesions. To clarify the cause–effect relationship among MMP-2 upregulation, BBB disruption, and WM lesions, we used 2 strategies to attenuate MMP-2 activity: an MMP inhibitor, AG3340, and MMP-2

Received March 2, 2006; final revision received June 9, 2006; accepted July 24, 2006.

From the Department of Neurology (K.N., M.I., R.T., H.T.), Horizontal Medical Research Organization (M.I.), the Department of Molecular Oncology (M.N.), and The 21st Century Center of Excellence Program, Department of Oncology (C.T.), Kyoto University Graduate School of Medicine, Kyoto, Japan; and the Laboratory for Behavioral Genetics (S.I.), RIKEN Brain Science Institute, Wako, Japan.

Correspondence to Kayoko Nakaji, MD, Department of Neurology, Graduate School of Medicine, Kyoto University, 54 Kawaharamachi, Shogoin, Sakyo-ku, Kyoto 606-8507, Japan. E-mail kann@kuhp.kyoto-u.ac.jp

© 2006 American Heart Association, Inc.

Stroke is available at http://www.strokeaha.org

DOI: 10.1161/01.STR.0000244808.17972.55

knockout. The results from both experiments strongly supported the idea that MMP-2 plays a critical role in BBB disruption and WM lesions.

Materials and Methods

Chronic Cerebral Hypoperfusion in Rats and Treatment With an Matrix Metalloproteinase Inhibitor

Chronic cerebral hypoperfusion with bilateral common carotid artery occlusion (BCAO) was induced in male Wistar rats (weight 150 to 200 g; Shimizu Experimental Supply; Kyoto, Japan) by double ligation of the common carotid arteries as previously described.[2] After the operation, the rats were kept in animal quarters with food and water ad libitum.

AG3340 (Agouron Pharmaceuticals) was dissolved at 75 mg/mL in 50% DMSO in propylenglycol. The rats were treated twice a day with an intraperitoneal injection of AG3340 (100 mg/kg) or vehicle (DMSO/propylenglycol) from just before the operation until 14 days after the operation. Similar doses and treatment paradigms have been shown to be effective in inhibiting MMP activity in gliomas in model animals.[9] Because our previous study demonstrated that the number of microglia peaked on 3 days and WM lesion started to become evident on 14 days after BCAO,[2] the animals were subjected to the analyses described subsequently.

Mice

The generation of C57BL/6J mice carrying the MMP-2-null allele has been described elsewhere.[10] In this mutant allele, a region containing the promoter and the first exon of the MMP-2 gene is replaced by the pgk-neo cassette. MMP-2$^{+/-}$ parents were mated to obtain both wild-type and MMP-2$^{-/-}$ (MMP-2-null) littermates. Genotyping was performed by polymerase chain reaction using the following primers: wild-type forward, CAACGATGGAGGCACGAGTG; wild-type reverse, GCCGGGGAACTTGATGATGG; mutant forward, CTTGGGTGGAGAGGCTATTC; and mutant reverse, AGGTGAGATGACAGGAGATC.

Chronic Cerebral Hypoperfusion in Mice and Cerebral Blood Flow Measurement

Adult male mice (weight 20 to 25 g) were subjected to bilateral common carotid arteries stenosis (BCAS) by applying the microcoils with an inner diameter of 0.18 mm to both common carotid arteries as previously described.[3] The cerebral blood flow (CBF) was recorded by laser Doppler flowmetry by placing a straight probe (OmegaFLO-N1; Neuroscience Inc) on 1 mm posterior and 2 mm lateral from bregma perpendicular to the skull bone through the guide cannula. The baseline CBF recordings were obtained just before and at 2 hours and 3, 7, 14, and 30 days after the surgery. The CBF values were expressed as a percentage of the baseline value.

Histochemical Evaluation of White Matter Lesions and Glial Activation

Under deep anesthesia, the animals were perfused with 10 mmol/L phosphate-buffered saline (300 mL for rats, 100 mL for mice) and then with a fixative consisting of 4% paraformaldehyde, 0.2% picric acid, and 0.1 mol/L phosphate buffer at pH 7.4 (300 mL for rats, 100 mL for mice). The brains were removed and postfixed for 24 hours in 4% paraformaldehyde in 0.1 mol/L phosphate buffer and then stored in 15% sucrose in 0.1 mol/L phosphate buffer. The fixed brains were embedded in paraffin and sliced into 2-μm-thick coronal sections. Klüver-Barrera staining and Bielschowsky staining were used to visualize the myelin sheaths and axons, respectively. As previously described,[2] the severity of the WM lesions was semiquantitatively graded as normal (grade 0), disarrangement of the nerve fibers (grade 1), formation of marked vacuoles (grade 2), and disappearance of myelinated fibers (grade 3) by an investigator blind to the experimental condition. For immunohistochemistry, serial sections (20-μm-thick) were cut in a cryostat and incubated overnight with a primary antibody at 4°C followed by incubation with the appropriate biotinylated secondary antibody (1 hour, room temperature), treatment with an avidin–biotin complex (diluted 1:200; Vector Laboratories), and visualization with 0.01% diaminobenzidine tetrahydrochloride and 0.005% H_2O_2 in 50 mmol/L Tris-HCl (pH 7.6). The primary antibodies used were as follows: monoclonal anti-rat glial fibrillary acidic protein (GFAP) (diluted 1:5000; Sigma-Aldrich; Mo, USA), polyclonal rabbit anti-mouse GFAP (diluted to 1:5000; Dako Cytomation, Denmark), polyclonal rabbit anti-MMP-2 (diluted to 1: 1,000, Chemicon International, Inc), monoclonal rat anti-mouse MHC class II antigen antibodies (diluted to 1:5000; Dako Cytomation), and rabbit anti Iba-1 antibody (1 μg/mL; Wako Pure Chemical Industries, Ltd; Osaka, Japan). Some sections were incubated with a biotinylated goat anti-rat IgM (μ), biotinylated goat anti-mouse IgM (μ) (diluted 1:1000; Kirkegaad & Perry Laboratories; Md, USA), or biotinylated Ricinus communis agglutinin-1 (diluted 1:1000; Vector Laboratories; Calif, USA) and were incubated directly with the avidin–biotin complex. To confirm the cellular source of IgM, sections were labeled by biotinylated anti-mouse IgM and rabbit anti-mouse GFAP followed by fluorescein isothiocyanate-labeled avidin (diluted 1:100; Dako Cytomation) and rhodamine-labeled goat anti- rabbit IgG (2.5 μL/mL; Dako). In the sections immunostained for Ricinus communis agglutinin-1, MHC class II antigen, Iba-1, GFAP, and IgM, we counted the number of immunopositive cells in at least 6 representative fields (per 0.25 mm^2) in the corpus callosum, the caudoputamen, and the optic tract for the quantitative analysis.

Zymography and Matrix Metalloproteinases-2 Activity Assay

Minced forebrain tissues were incubated with gentle rotation at 4°C for 20 hour in an extraction buffer consisting of 0.5% Triton-X 100, 0.5 U/mL aprotinin, and 0.01% sodium azide in 0.01 mol/L phosphate-buffered saline. The samples were then centrifuged at 14 000 rpm for 15 minutes at 4°C and the supernatants were collected. The protein content was adjusted to 10 mg/mL. The gelatinolytic activity of these samples was detected by SDS-PAGE zymography as described elsewhere,[8] although MMP-2 activity in the gray matter may interfere a sensitive detection of the activity in the WM. Equal amounts of tissue extract (50 μg) were then subjected to electrophoresis. To restore the activity of the protein, sample gels were agitated in 0.01 mol/L Tris-HCl (pH 8.0) containing 2.5% Triton X-100 (30 minutes×2). After washed in 0.05 mol/L Tris-HCl (pH 8.0) for 30 minutes, the gels were incubated overnight twice at 37°C in 0.05 mol/L Tris-HCl (pH 8.0) containing 0.5 mmol/L $CaCl_2$ and 1.0 mol/L $ZnCl_2$. After incubation, the gels were stained with Coomassie blue R-250. The amount of activated and latent forms of MMP-2 in the whole forebrain extracts were also assessed using the Matrix Metalloproteinase-2 Biotrak Activity Assay System (Amersham Biosciences), which is based on a 2-site enzyme-linked immunosorbent assay "sandwich" format and recognizes both the proform and active form of MMP-2.

Evans Blue Extravasation

The mice were killed at 3 hours and 1, 3, 5, 7, and 14 days after BCAS. One hour before each time point, 1 mL of 4% Evans blue (EB; Nakalai Chemicals Ltd) in normal saline was injected intraperitoneally. The animals were anesthetized and then perfused transcardially with 200 mL of 10 mmol/L phosphate-buffered saline. The brains were snap-frozen, sectioned into 20-μm-thick slices, and examined by fluorescence microscopy. For quantitative measures, the images were analyzed within 4 structurally similar areas (2 paramedian portions of the corpus callosum on each hemisphere) in each mouse and digitally level-adjusted by Adobe Photoshop (Adobe Systems) so that intravascular EB would be reported as white (pixel value 255) on a black background (pixel value 0). Using the public domain NIH Image 1.61 program (National Institutes of Health), the images were then binarized with intensity threshold set at pixel value 50 so that the white pixels represent intravascular and extravasated EB. The number of white pixels was divided by the total pixel

number in the selected area to estimate percent area containing intravascular and extravasated EB as an approximate index of BBB breakdown. Image analysis was focused on the paramedian portion of the corpus callosum facing the dorsal part of the lateral ventricle, because WM lesions were most intense in this region.[3]

Statistical Analysis

All data are presented as means±SE. A one-factor ANOVA followed by Fisher protected least significant difference procedure was used to compare the differences between groups. P values <0.05 were considered to be statistically significant.

Results

The amount of total MMP-2 in the forebrain extracts was comparable between the vehicle-treated and AG3340-injected rats after BCAO as assessed using the Biotrak Activity Assay System. The percentage of activated MMP-2 was only 7% on day 3 after the sham operation but was elevated to approximately 80% on day 3 after the BCAO (supplemental Figure I, available online at http://stroke.ahajournals.org). We also confirmed almost complete suppression of MMP-2 activation with AG3340 administration.

The operation was successful in rats (n=40) except 3, which developed convulsions and was killed within 7 days, and in mice (n=62) except 4, which developed cerebral infarction. These animals with unsuccessful operations were excluded from the statistical analysis. In the vehicle-treated animals, severe WM lesions, as shown by an increased number of disarranged nerve fibers and vacuolation, were found on day 14 after the BCAO in the optic nerve, medial part of the corpus callosum (Figure 1B and 1E), the internal capsule, and the fiber bundles of the caudoputamen. In such WM regions, the number of Ricinus communis agglutinin-1-positive microglia and GFAP-positive astroglia increased (2- to 3-fold) on day 3 after the BCAO (Figure 1H and 1K). Both WM lesions and gliosis were less severe in the AG3340-treated animals (Figure 1C, 1F, 1I, 1L, 1P through 1R, and Table 1).

The BBB integrity in rats subjected to BCAO was also assessed by the immunostaining for IgM. IgM-immunoreactive glial cells represent those cells that have taken up the serum proteins, which leaked into the brain parenchyma, and their number serves as an indicator of BBB dysfunction.[8] Some IgM-immunoreactive glial cells were found in the vicinity of the microvessels in the corpus callosum in the vehicle-treated animals on day 3 after the BCAO (Figure 1R), suggesting BBB dysfunction in this region. In contrast, much fewer IgM-immunoreactive glia were found in the same area of the AG3340-treated animals (Figure 1O and 1R).

These results strengthen the notion that MMPs play a role in BBB impairment and WM lesions. To further elucidate the roles of MMPs in the WM damage after chronic cerebral hypoperfusion, we applied BCAS (the established technique for mice hypoperfusion)[3] for mice lacking functional MMP-2 gene (MMP-2-null mice), which showed no obvious developmental abnormalities[10] or brain anomalies[11] and examined its effects using histochemical methods. The reduction of CBF after BCAS was comparable between wild-type and MMP-2-null mice. The CBF reductions (wild-type versus MMP-2-null; mean±SE %, n=3 each) were 42.5±4.3% versus 39.1±3.2% (2 hours after BCAS), 38.1±4.3 versus 39.4±4.0 (3 days), 35.2±4.6 versus 33.6±6.2 (7 days), 20.8±1.4 versus 26.9±3.1 (14 days), and 11.2±3.0 versus 24.0±4.0 (30 days). In wild-type mice, MMP-2-immunoreactive glial cells increased after BCAS compared with sham-operated mice (Figure 2A and 2B). MMP-9-immunoreactive cells were not induced after BCAS in both wild-type (Figure 2C and 2D) and MMP-2-null mice (Figure 2E). Consistently, zymography using forebrain homogenates revealed only a faint band of MMP-9 in the samples after BCAS for 3 days in both wild-type and MMP-2-null mice (n=4), whereas a robust band was found in the sample from a mouse with an incidental cerebral infarction after BCAS (Figure 2G). A band of MMP-2 was detected in the samples in wild-type mice but not in MMP-2-null mice after BCAS (n=4). However, zymography using such homogenates failed to show the upregulation of MMP-2 after 3 days of BCAS; regional upregulation of MMP-2 in the WM seemed obscured.

Klüver-Barrera staining revealed that WM lesions were predominant in the corpus callosum, caudoputamen, and internal capsule but not in optic tract on day 30 after BCAS in the wild-type mice. The medial part of the corpus callosum adjacent to the lateral ventricles was most severely affected (Figure 3E). In MMP-2-null mice, such WM lesions were far less severe (Figure 3I; Table 2). The mouse model showed little damage to the visual pathway and no difference was found between the wild-type mice and MMP-2-null mice after the operation. This may be attributable to the fact that BCAS in mice induces a milder decrease in the CBF than in the rat model and maintains a residual blood flow within the common carotid arteries and its branch, the ophthalmic artery.

In the wild-type mice on day 14 after BCAS, numerous activated microglia, as visualized by immunostaining with anti-MHC class II antibodies, were found in some WM regions (Figure 3F). In addition, the number of GFAP-immunoreactive astroglia increased in these mice (Figure 3G). In the MMP-2-null mice, the number of microglia and astroglia was much fewer in the WM as compared with the wild-type animals (Figure 3J, 3K, 3P, 3Q). Thus, both WM lesions and glial activation after chronic hypoperfusion were dramatically reduced in the MMP-2-null mice. There was no difference of the number of microglia, astroglia, and IgM-positive cells in optic tract (Figure 3P).

The BBB integrity in mice subjected to BCAS was assessed by the immunostaining for IgM and EB extravasation assay. After BCAS, the number of IgM-positive cells increased in the WM of the wild-type mice (Figure 3H) as compared with the sham-operated wild-type animals (Figure 3D). Intriguingly, the IgM-immunoreactive cells significantly decreased in the WM of MMP-2-null mice after BCAS (Figure 3L and 3R). IgM-immunoreactive cells were identified as astroglia based on their colabeling with GFAP in the perivascular areas (Figure 3L through 3O). Three days after BCAS, EB apparently leaked into the perivascular area in the corpus callosum (Figure 4B) and the cerebral cortex (data not shown). This extravasation was most notable in the paramedian portion of the corpus callosum. At all time points after BCAS, no extravasation of EB could be detected in the MMP-2-null mice (Figure 4C). The estimated percent area

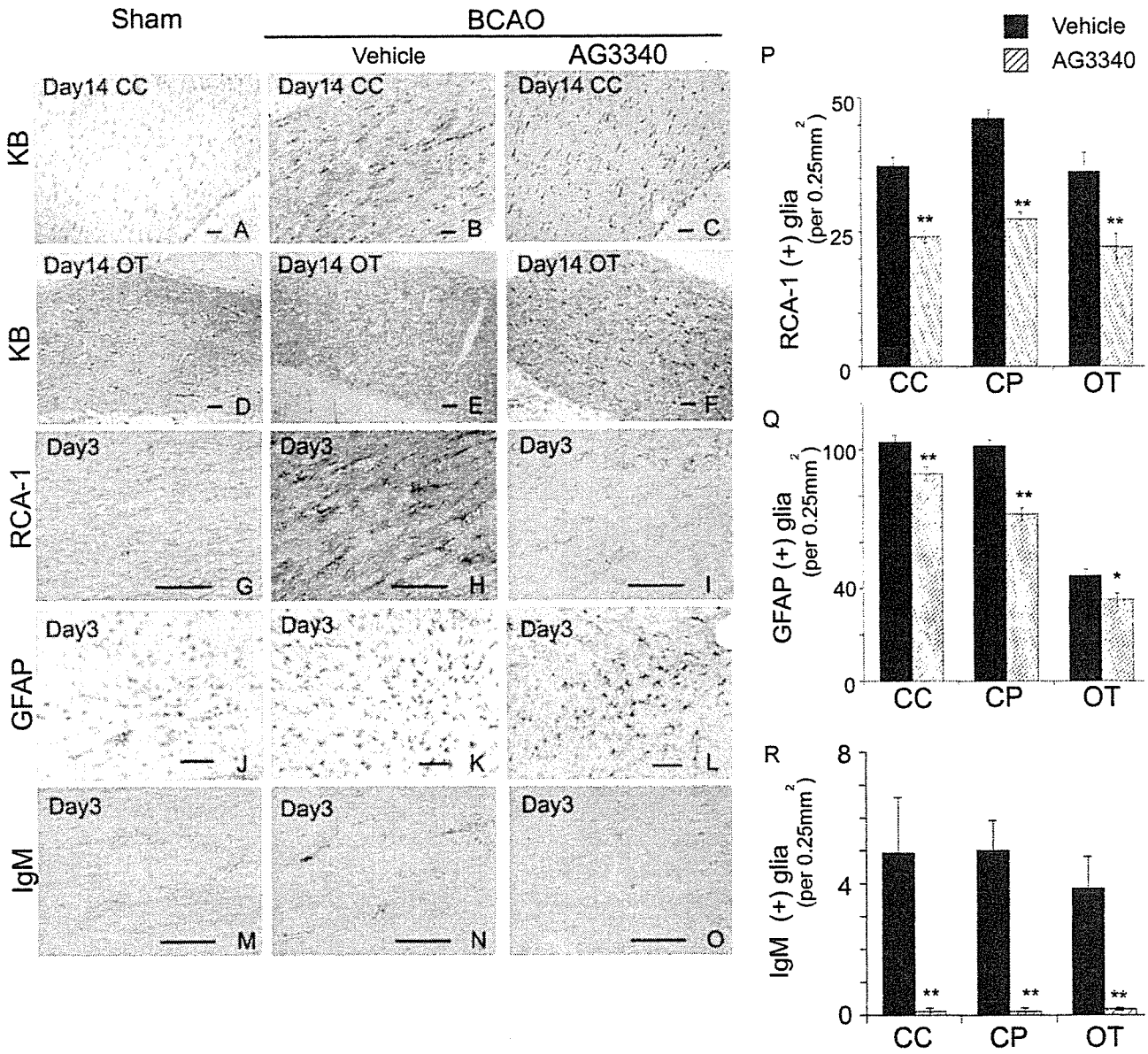

Figure 1. Histologic evaluation of the WM lesions in rats after chronic cerebral hypoperfusion with or without AG3340-treatment. A through O, Klüver-Barrera staining on day 14 (A through F; myelin sheath) or immunostaining on day 3 for Ricinus communis agglutinin-1 (G through I; microglia), GFAP (J through L; astroglia), or IgM (M through O) of the corpus callosum (A through C, G through O) and optic tract (D through F) of rats that had undergone sham operation (A, D, G, J, M) or BCAO operation, which had been treated either with vehicle (B, E, H, K, N) or AG3340 (C, F, I, L, O). Scale bar, 50 μm. (P through R) A histogram representing the density of cells immunoreactive for Ricinus communis agglutinin-1 (P), GFAP (Q), or IgM (R) in sections from the corpus callosum (CC), caudoputamen (CP), and optic tract (OT) in rats 3 days after a BCAO (n=4 each; *P<0.05, **P<0.01).

stained with EB was approximately 8% in wild-type mice after BCAS, which significantly reduced to 2% in MMP-2-null mice after BCAS (Figure 4D). Taken together, these results indicated that loss of MMP-2 alleviated BBB damage after BCAS and suggested a causative role for MMP-2 in the WM lesions after hypoperfusion.

TABLE 1. Histologic Grading of the WM Lesions in Untreated and AG3340-Treated Rats on Day 14 After BCAO

	Corpus Callosum	Caudoputamen	Optic Tract
Vehicle, N=5	1.3±045	1.4±0.54	2.6±0.55
AG3340, N=4	0.5±0.4*	0.63±0.25*	1.13±0.63*

*P<0.05.

Discussion

The synthetic MMP inhibitor AG3340 is known to inhibit several MMP family members, including MMP-2 (Ki=0.05 nmol/L), MMP-9 (0.26 nmol/L), MMP-13 (0.03 nmol/L), and MT1-MMP (0.33 nmol/L).[12] As a lipophilic, low-molecular-weight (Mr 423.5) compound, AG3340 can readily cross the BBB.[12] Using this compound, we have demonstrated that AG3340 shows protective effects against the WM lesions after chronic cerebral hypoperfusion in rats. This is consistent with our previous data using the same model, which showed a correlation of WM lesions with MMP-2 upregulation.[8] Then, AG3340 may have reduced the severity of WM lesions by inhibiting MMP-2 activation. In support of this notion,

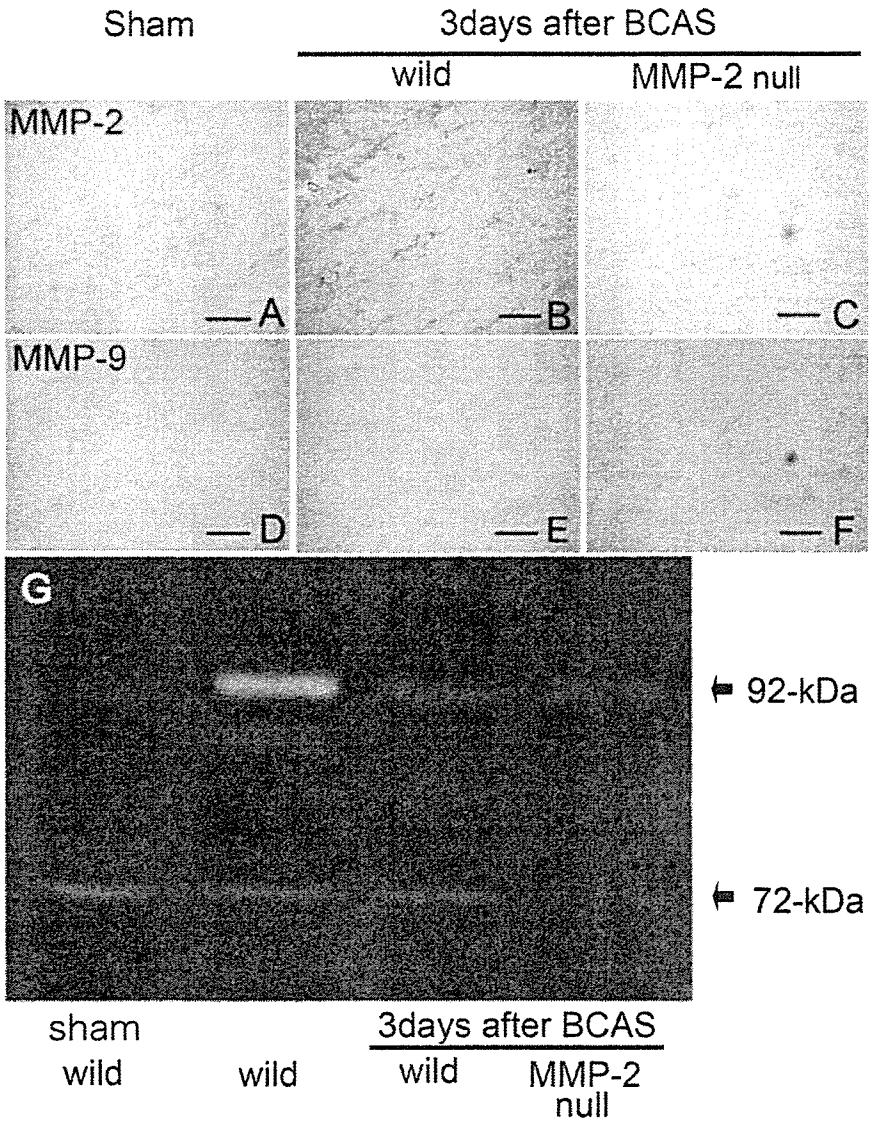

Figure 2. A through F, Immunohistochemical analysis for MMP-2 (A through C) and MMP-9 (D through F) in the corpus callosum of wild-type mice (A, B, D, E) or MMP-2-null mice (C, F) on day 3 after sham operation or BCAS (B, D). G, Zymography assay of the samples from a mouse with incidental cerebral infarction (CI), a wild-type mouse and an MMP-2-null mouse 3 days after BCAS. Note the absence of compensatory upregulation of MMP-9 in MMP-2-null mice.

genetic deletion of MMP-2 attenuated the WM lesions after chronic cerebral hypoperfusion in mice. These data jointly suggest that MMP-2 upregulation plays a major role in the WM lesions.

Previous studies have established the importance of the upregulation and activation of MMPs in acute brain ischemia.[13–15] Among the members of the MMP family (n≥20), MMP-9 is of particular interest in the context of acute brain ischemia, because the selective upregulation of MMP-9 has been observed in the brains of patients with stroke.[15] More importantly, the neuronal damage after cerebral ischemia was attenuated in the MMP-9-null mice compared with the wild-type mice.[16] Furthermore, Heo et al demonstrated association of MMP-9 upregulation with hemorrhagic transformation in the nonhuman primates.[17] Thus, MMP-9 upregulation may contribute to the BBB damage and infarct size, especially in the acute setting. Although previous study demonstrated the upregulation of MMP-9 in MMP-2-null mice,[18] no upregulation of MMP-9 was observed in our model, which suggested a negligible role of MMP-9 in chronic cerebral hypoperfusion.

What then would be the role of MMPs in cerebral ischemia? Hamann et al reported disappearance of the basal lamina around the microvessels during cerebral ischemia and reperfusion.[7] Fukuda et al demonstrated that the ischemic primate brain contained elevated levels of activity enough to digest basal lamina components such as type IV collagen.[19] In fact, Heo et al indicated that MMP-2 upregulated significantly by 1 hour after MCAO[18] and was persistently elevated thereafter in primates, and Chan et al demonstrated the upregulation of activation system for latent MMP-2 after focal cerebral ischemia.[20] These findings support the hypothesis that excessive degradation of the vascular basal lamina is a mechanism by which MMP triggers BBB dysfunction, edema, hemorrhage. The most marked extravasation of Evans blue in the paramedian portion of the corpus callosum facing the lateral ventricle was consistent with a previous report on a rat model of chronic cerebral hypoperfusion[21] and further indicated a vulnerability of the BBB in this area. In the case of chronic hypoperfusion, a previous study suggested the association of MMP-2 but not MMP-9 upregulation with BBB disruption. Consistently, Rosenberg et al showed that the activated

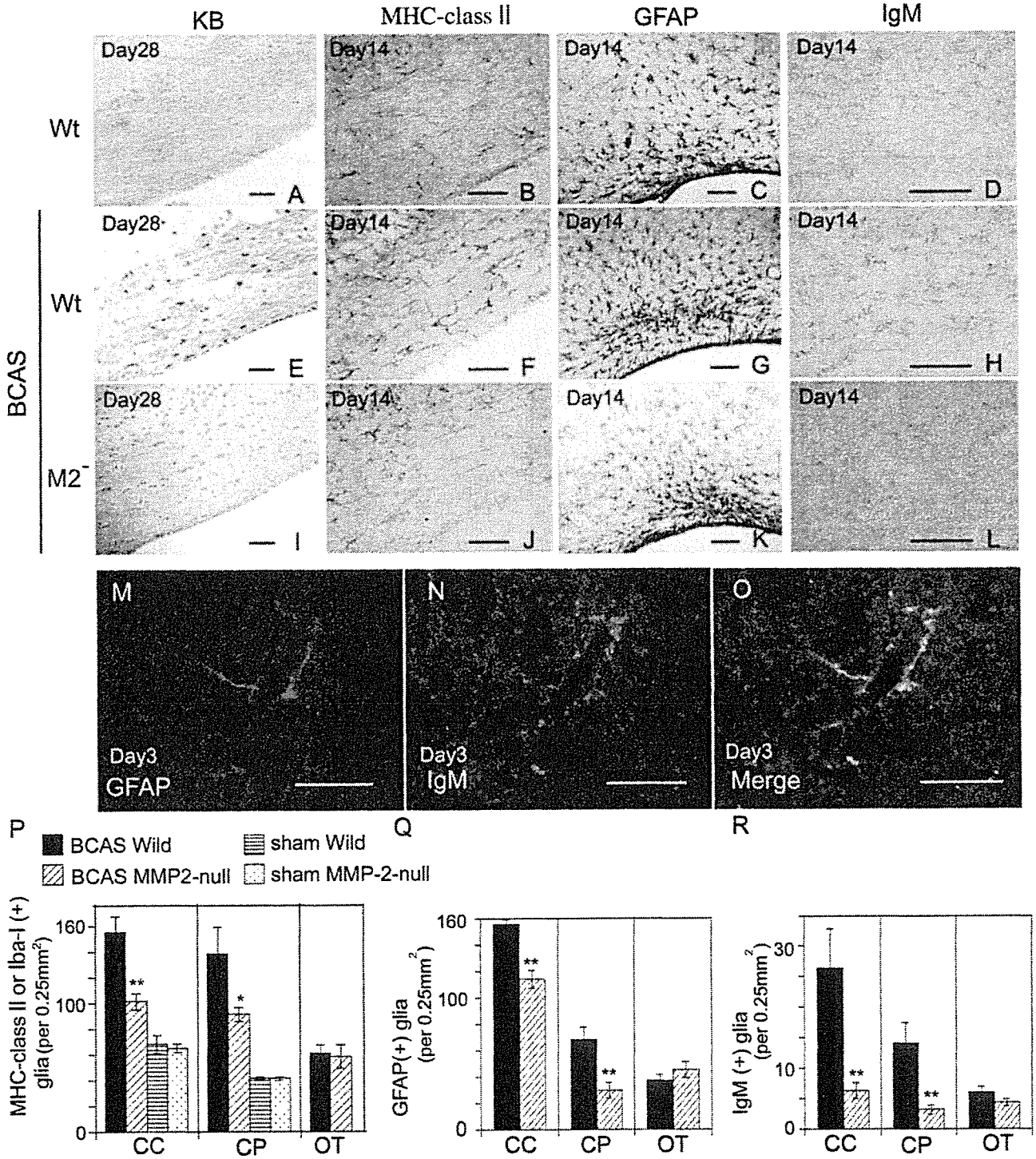

Figure 3. Histologic evaluation of the WM lesions in wild-type and MMP-2-null mice after BCAS. A through L, Klüver-Barrera staining 28 days after BCAS (A, E, I) and immunostaining 14 days after BCAS for MHC class II (B, F, J), GFAP (C, G, K), or IgM (D, H, L) of corpus callosum sections from wild-type (Wt) mice (A through H) or MMP-2-null ($M2^-$) mice (I through L) that had undergone either a sham operation (A through D) or BCAS (E through L). Note that MMP-2 gene knockout recover the decrease of Klüver-Barrera staining in the WM after BCAS (compare E with I) and glial activation (compare F with J for microglia and G with K for astroglia). Scale bar, 50 μm. M through O, Double staining with GFAP and IgM of the WM lesions in wild-type mice after BCAS. IgM was observed on endfeet of GFAP-positive glia (O). Scale bar, 10 μm. P through R, A histogram representing the density of cells immunoreactive for MHC-class II or Iba-I (P), GFAP (Q), or IgM (R) in sections from the corpus callosum (CC), caudoputamen (CP), and optic tract (OT) of mice that had undergone BCAS (n=6 each; $^*P<0.05$, $^{**}P<0.01$). For the microglial count, anti-MHC-class II antibodies were used for mice with BCAS operation, whereas anti-Iba-I antibodies were used for mice with sham operation (P). Note that glial activation was not observed in the optic tract, being consistent with the absence of rarefaction of this structure.

TABLE 2. Histologic Grading of the WM Lesions in Wild-Type and MMP-2-Null Mice on Day 30 After BCAS

	Corpus Callosum	Caudoputamen	Anterior Commissure
Wild-type, N=6	1.5±0.8	1.3±0.58	0.5±0.5
MMP-2-null, N=6	0.5±0.8*	0.58±0.37*	0±0

*$P<0.05$.

astroglia and microglia/macrophages around the arterioles expressed MMP-2 and MMP-3, but not MMP-9, in the brains of patients with vascular dementia.[6]

Caplan[22] proposed that the major pathologic features of WM lesions such as demyelination and gliosis may result from a BBB dysfunction, which allows the leakage of proteins and fluid through the compromised barrier of the penetrating arteries. This hypothetical pathway is consistent with our present findings. Given the overlapping substrate specificity between MMP-2 and MMP-9, in the case of chronic cerebral hypoperfusion, MMP-2 may contribute to the BBB disruption through the excessive digestion of the vascular basal lamina and activation of glia. In addition, MMP-2 may be directly involved in demyelination associated with WM lesions, because MMP-2 can digest myelin more efficiently than MMP-9.[24]

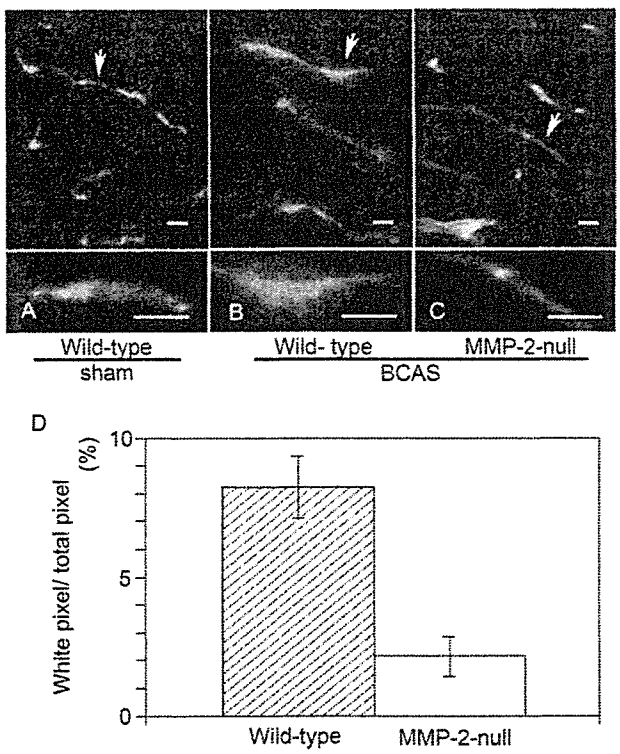

Figure 4. Evaluation of BBB dysfunction in the corpus callosum of mice. The Evans blue extravasation assay was performed on day 3 after a sham operation in wild-type mice (A) or on day 3 after BCAS in wild-type (B) and MMP-2-null mice (C). A magnified view of the area indicated by an arrow in the upper panel is shown in the lower panel (A through C). The experiments were repeated in triplicate with similar findings (n=4 each). Scale bar, 100 μm. A histogram representing the degree of Evans blue extravasation as an approximate index of BBB breakdown (see "Methods") (D).

In conclusion, the present study has provided direct evidence that MMP-2 is involved in the pathogenesis of WM lesions in the mouse model. Although the species difference between rodents and humans should be taken into consideration, our data also suggest the potential value of MMP inhibitors in preventing subcortical ischemic vascular dementia resulting from BBB dysfunction and chronic cerebral ischemia in humans. Activation of MMP-2 is reported to participate in matrix injury during focal cerebral ischemia. An elucidation of the exact roles of MMP-2 in BBB disruption may also provide information useful in developing strategies for controlling neuroinflammation in general.

Acknowledgments

The authors are indebted to Miss Nakabayashi for her excellent technical assistance.

Disclosures

None.

References

1. Meguro K, Hatazawa J, Yamaguchi T, Itoh M, Matsuzawa T, Ono S, Miyazawa H, Hishinuma T, Yanai K, Sekita Y. Cerebral circulation and oxygen metabolism associated with subcortical perivascular hyperintensity as shown by magnetic resonance imaging. *Ann Neurol.* 1990;28:378–383.
2. Wakita H, Tomimoto H, Akiguchi I, Kimura J. Glial activation and white matter changes in the rat brain induced by chronic cerebral hypoperfusion: an immunohistochemical study. *Acta Neuropathol.* 1994;87:484–492.
3. Shibata M, Ohtani R, Ihara M, Tomimoto H. White matter lesions and glial activation in a novel mouse model of chronic cerebral hypoperfusion. *Stroke.* 2004;35:2598–2603.
4. Sternlicht MD, Werb Z. How matric metalloproteinases regulate cell behavior. *Annu Rev Cell Dev Biol.* 2001;17:463–516.
5. Clark AW, Krekoski CA, Bou SS, Chapman KR, Edwards DR. Increased gelatinase A (MMP-2) and gelatinase B (MMP-9) activities in human brain after focal ischemia. *Neurosci Lett.* 1997;238:53–56.
6. Rosenberg GA, Sullivan N, Esiri MM. White matter damage is associated with matrix metalloproteinases in vascular dementia. *Stroke.* 2001;32:1162–1168.
7. Hamann GF, Okada Y, Fitridge R, del Zoppo GJ. Microvascular basal lamina antigens disappear during cerebral ischemia and reperfusion. *Stroke.* 1995;26:2120–2126.
8. Ihara M, Tomimoto H, Kinoshita M, Oh J, Noda M, Wakita H, Akiguchi I, Shibasaki H. Chronic cerebral hypoperfusion induces MMP-2 but not MMP-9 expression in the microglia and vascular endothelium of the white matter. *J Cereb Blood Flow Metab.* 2001;21:828–834.
9. Price A, Shi Q, Morris D, Wilcox ME, Brasher PM, Rewcastle NB, Shalinsky D, Zou H, Appelt K, Johnston RN, Yong VW, Edwards D, Forsyth P. Marked inhibition of tumor growth in a malignant glioma tumor model by a novel synthetic matrix metalloproteinase inhibitor AG3340. *Clin Cancer Res.* 1999;4:845–854.
10. Itoh T, Ikeda T, Gomi H, Nakao S, Suzuki T, Itohara S. Unaltered secretion of beta-amyloid precursor protein in gelatinase A (matrix metalloproteinase 2)-deficient mice. *J Biol Chem.* 1997;272:22389–22392.
11. Asahi M, Sumii T, Fini ME, Itohara S, Lo EH. Matrix metalloproteinase 2 gene knockout has no effect on acute brain injury after focal ischemia. *Neuroreport.* 2001;12:3003–3007.
12. Shalinsky DR, Brekken J, Zou H, McDermott CD, Forsyth P, Edwards D, Margosiak S, Bender S, Truitt G, Wood A, Varki NM, Appelt K. Broad antitumor and antiangiogenic activities of AG3340, a potent and selective MMP inhibitor undergoing advanced oncology clinical trials. *Ann N Y Acad Sci.* 1999;878:236–270.
13. Rosenberg GA, Navratil M, Barone F, Feuerstein G. Proteolytic cascade enzymes increase in focal cerebral ischemia in rat. *J Cereb Blood Flow Metab.* 1996;16:360–366.

14. Horstmann S, Kalb P, Koziol J, Gardner H, Wagner S. Profiles of matrix metalloproteinases, their inhibitors, and laminin in stroke patients: influence of different therapies. *Stroke*. 2003;34:2165–2170.
15. Maier CM, Hsieh L, Yu F, Bracci P, Chan PH. Matrix metalloproteinase-9 and myeloperoxidase expression: quantitative analysis by antigen immunohistochemistry in a model of transient focal cerebral ischemia. *Stroke*. 2004; 5:1169–1174.
16. Lee SR, Tsuji K, Lee SR, Lo EH. Role of matrix metalloproteinase in delayed neuronal damage after transient global ischemia. *J Neurosci*. 2004;24:671–678.
17. Heo JH, Lucero J, Abumiya T, Koziol JA, Copeland BR, del Zoppo GJ. Matrix metalloproteinases increase very early during experimental focal cerebral ischemia. *J Cereb Blood Flow Metab*. 1999;19:624–633.
18. Esparza J, Kruse M, Lee J, Michaud M, Madri JA. MMP-2 null mice exhibit an early onset and severe experimental autoimmune encephalomyelitis due to an increase in MMP-9 expression and activity. *FASEB J*. 2004;18:1682–1691.
19. Fukuda S, Fini CA, Mabuchi T, Koziol JA, Eggleston LL Jr, del Zoppo GJ. Focal cerebral ischemia induces active proteases that degrade microvascular matrix. *Stroke*. 2004;35:998–1004.
20. Chang DI, Hosomi N, Lucero J, Heo JH, Abumiya T, Mazar AP. Activation system for latent matrix metalloproteinase-2 are upregulated immediately after focal cerebral ischemia. *J Cereb Blood Flow Metab*. 2003;23:1408–1419.
21. Ueno M, Tomimoto H, Akiguchi I, Wakita H, Sakamoto H. Blood–brain barrier disruption in white matter lesions in a rat model of chronic cerebral hypoperfusion. *J Cereb Blood Flow Metab*. 2002; 22:97–104.
22. Caplan LR. Dilatative arteriopathy (dolichoectasia): what is known and not known. *Ann Neurol*. 2005;57:472–479.
23. Chandler S, Coates R, Gearing A, Lury J, Wells G, Bone E. Matrix metalloproteinases degrade myelin basic protein. *Neurosci Lett*. 1995; 201:223–226.

ELSEVIER

Journal of the Neurological Sciences 251 (2006) 129–133

Journal of the Neurological Sciences

www.elsevier.com/locate/jns

Short communication

Heterogeneous epileptogenicity and cortical function within malformations of cortical development: A case report

Masako Kinoshita [a], Akio Ikeda [a,*], Junya Taki [b], Keiko Usui [c], Riki Matsumoto [a], Nobuhiro Mikuni [b], Jun B. Takahashi [b], Hidenao Fukuyama [c], Nobuo Hashimoto [b], Ryosuke Takahashi [a]

[a] *Department of Neurology, Graduate School of Medicine, Kyoto University, 54 Shogoin-Kawaharacho, Sakyoku, Kyoto, 606-8507, Japan*
[b] *Department of Neurosurgery, Graduate School of Medicine, Kyoto University, 54 Shogoin-Kawaharacho, Sakyoku, Kyoto, 606-8507, Japan*
[c] *Human Brain Research Center, Graduate School of Medicine, Kyoto University, 54 Shogoin-Kawaharacho, Sakyoku, Kyoto, 606-8507, Japan*

Received 30 December 2005; received in revised form 19 July 2006; accepted 11 September 2006
Available online 13 November 2006

Abstract

The authors report a 24-year-old patient with intractable partial epilepsy and massive malformations of cortical development (MCD). Subdural EEG recordings of habitual seizures showed heterogeneous epileptogenicity, and visual evoked potential was recorded within the MCD just adjacent to the most active epileptogenic focus. Resection of the small cortical area presumably with core epileptogenicity, while sparing the cortical functional area, improved seizure outcome without any postoperative functional deficits.
© 2006 Elsevier B.V. All rights reserved.

Keywords: Epileptogenicity; Cortical function; Malformations of cortical development; Visual evoked potential; Subdural EEG record; Epilepsy surgery

1. Introduction

Malformations of cortical development (MCDs) are present in 15–20% of adult patients with intractable partial epilepsy [1]. However, epileptogenicity within MCD varies within as well as among individuals: epileptic activities correlate with in situ histopathologic patterns in MCD [2]. Several case reports have suggested a possibility that partial resection of MCD can give a good seizure outcome [3,4] although generally the best seizure control has been achieved when complete or major excision of both the MRI-visible lesion and the cortical areas generating ictal electrographic activity [4,5]. Recent case reports and imaging studies have shown that cortices showing MCD have normal brain functions [6–9], and therefore, resection of MCD may carry a potential risk of neurological functional deficits.

Here we report a patient with partial seizures caused by MCD which had heterogeneous epileptogenicity and visual function delineated by presurgical evaluation using subdural electrodes. The most active epileptogenic area and visual functional area resided side by side within MCD. After resection of the small area of the most active epileptogenicity, the seizures significantly decreased with no functional deficits in spite of large residual MCD.

2. Patient and methods

2.1. Case presentation

A 24-year-old right-handed woman with medically intractable partial seizures had implanted subdural electrodes for presurgical evaluation. All the clinical procedures were done after full explanation about the methods and possible side effects to the patient and her family, according to clinical research protocol approved by the Ethical Committee of

* Corresponding author. Tel.: +81 75 751 3772; fax: +81 75 751 9416.
E-mail address: akio@kuhp.kyoto-u.ac.jp (A. Ikeda).

0022-510X/$ - see front matter © 2006 Elsevier B.V. All rights reserved.
doi:10.1016/j.jns.2006.09.016

Kyoto University Graduate School of Medicine (No. 79). She developed complex partial seizures (CPSs) when she was 17 years old. Her habitual seizures started with auras consisting of a sensation that something was rising from her feet and/or auditory hallucination of high-pitched sound, developed to CPSs with oral (chewing) and bilateral hand automatisms, followed by postictal cough. She had no personal or familial antecedents for epilepsy. Neurological examination showed left lower homonymous quadrianopsia. Her seizures were intractable in spite of administration of multiple drugs such as phenytoin, carbamazepine, phenobal and clobazam of appropriate dose.

An MRI revealed massive MCDs including schizencephaly and polymicrogyria in the right temporo-parieto-occipital area (Fig. 1A-D). By non-invasive video-EEG monitoring during habitual seizures consisted of motion arrest, staring, oral and hand automatisms, ictal discharges started with low-voltage fast activities at the right posterior temporal area before the clinical onset. Interictal FDG-PET showed heterogeneous regional glucose hypometabolism in the right temporo-occipital area (Fig. 1E), and ictal SPECT showed an increased perfusion in that area (Fig. 1F). Intracarotid propofol test [10] revealed language and memory dominance in the left hemisphere.

2.2. Presurgical evaluation with subdural electrodes

The electrodes were disks of 3.0 mm diameter made of platinum–iridium (Ad-Tech, Racine, WI, U.S.A.), placed with center-to-center distance of 1 cm within the silicon rubber sheet. Two sheets of 4×5 subdural electrode grid, one each on the right parietal and temporal lobes, and one 1×4 subdural electrode strip on the right temporal lobe were implanted. One set of depth electrodes made of platinum, 1.5 mm diameter, 4-contact of 1.0 mm length, with 5 mm spacing (UNIQUE MEDICAL, Tokyo, Japan), was inserted into the right antero-temporal area. The epileptogenic area was determined by simultaneous monitoring of video and subdural EEG during the patient's habitual clinical seizures.

Functional mapping was performed with the left median and tibial somatosensory evoked potential (SEP), auditory evoked potential (AEP) and visual evoked potential (VEP)

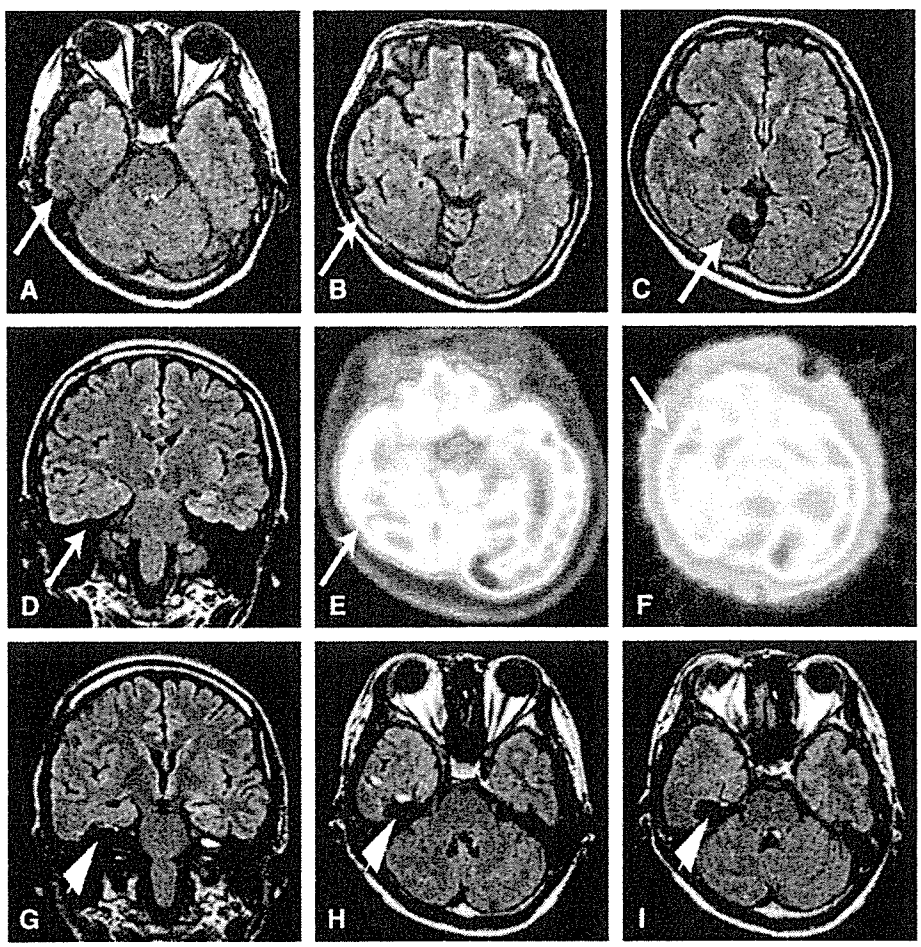

Fig. 1. Preoperative brain MRI (A–D), interictal FDG-PET (E), ictal SPECT (F) and postoperative brain MRI (G–I). (A–D) Massive MCD including a schizencephaly and polymicrogyria in the right temporo-parieto-occipital area (arrows). (E) Heterogeneous regional glucose hypometabolism in the right temporo-occipital area. (F) Ictal SPECT showed an increased perfusion in that area. (G–I) Small area with the most active epileptogenicity was resected (arrowhead). The patient showed reduction of seizures (Engel's class IIA) in spite of a large residual lesion.